Chapter 5

Kalman filter double deconvolution method

5.1 Introduction

The forward and single deconvolution calculations described in the previous chapter use $\delta^{13}C$ for validation. In contrast, double deconvolution calculations use $\delta^{13}C$ much more directly. Previous double deconvolutions (e.g., Joos and Bruno, 1998; Francey et al., 1995b) have used the change in CO_2 and $\delta^{13}C$ through time to solve for the budgets of CO_2 and $^{13}CO_2$, requiring CO_2 and $\delta^{13}C$ to be known at every time step. This is well suited to studies over recent years, where direct measurements give good temporal coverage. For longer time scales, smoothing spline fits to ice core data are generally used, however assumptions about the degree of smoothing on the splines can have important implications for the inferred sources and their variability.

In this chapter, an alternative double deconvolution method will be developed and applied to the Law Dome ice core record. The method, which uses the Kalman filter, incorporates statistical analysis into the carbon cycle modelling. The statistics are used in parallel with the carbon cycle modelling, in contrast to the Bayesian calibration of the BDM in Chapter 4 which implemented the statistical analysis as an external shell. An important feature of the Kalman filter inversion is that estimates of the uncertainties in the deduced sources, as well as the sources themselves, are readily calculated. The concepts of state space modelling and the application of Kalman filtering to ice core records will first be demonstrated using the Law Dome methane ice core record. This provides an example that is easier to understand than the double deconvolution of CO_2 and $\delta^{13}C$, yet has many

of the same issues. The methane example is also interesting in its own right.

The outline of this chapter is as follows. The equations for the Kalman filter and some extensions (smoothing algorithms and the Extended Kalman filter for nonlinear problems) are explained, with a methane example used to illustrate the linear methods. A discussion of some previous applications of Kalman filtering to trace gas studies is then given, followed by a discussion of the methane results. The next section is on testing the statistics in the methane example, and raises some issues that will be important for the CO_2 calculations. The Kalman filter is then applied to the Law Dome CO_2 and $\delta^{13}C$ records. A simple approach using the Kalman filter with atmospheric pulse response functions is described first. This approach has a number of limitations due to over-simplification, but is quite valuable to illustrate the methods. A more complete, nonlinear solution using mixed layer pulse response functions is then applied to the double deconvolution of CO_2 and $\delta^{13}C$. The results are compared to the traditional mass balance double deconvolution method. A list of the notation used in this chapter is given in Appendix 5-1.

5.2 Methods

5.2.1 The Kalman filter

Kalman filtering is a recursive algorithm derived by Kalman (1960) for the discrete case and Kalman and Bucy (1961) for the continuous case. The method aims to produce estimates of the *state* of a system at each timestep using a state-space model. The concept of a state is important here. Gabel and Roberts (1973) give the definition 'The state of a system at time t is that (minimal) set of variables needed at time t so that, given the inputs to the system for $\tau > t$, one can exactly specify the future behaviour of the system for $\tau > t$'. (It is sometimes desirable for the state to include more than the 'minimal' required set of variables, for example to include secondary variables for which estimates are sought.) Basically, the Kalman filter consists of predicting the state at each timestep from the state at the previous timestep, with improvements to the estimates made using (noisy) measurements. The error covariance of the state is also predicted and updated. The Kalman filter is called a filter because it aims to reduce the influence of noise in the measurements (Mulquiney et al., 1993). A good description of Kalman filtering is given by Gelb (1974).

The model underlying the Kalman filter is given by two equations

$$\mathbf{x}_k = \Phi_{k-1}\mathbf{x}_{k-1} + \mathbf{G}_{k-1}\mathbf{u}_{k-1} + \mathbf{w}_{k-1} \tag{5.1}$$

$$\mathbf{z}_k = \mathbf{H}_k\mathbf{x}_k + \mathbf{v}_k \tag{5.2}$$

Equation (5.1) describes the evolution of the state from one time to the next, where $\mathbf{x}_k$ is the state at time k, Φ_k is the evolution (or transition) matrix and $\mathbf{G}_k\mathbf{u}_k$ is a deterministic forcing term. $\mathbf{w}_k$ is the stochastic forcing, which is assumed to be white noise with zero mean and covariance $\mathbf{Q}$. Equation (5.2) describes projection of the state onto observations, where $\mathbf{z}_k$ are observations at time k, and $\mathbf{H}_k$ is the projection (or measurement) matrix. $\mathbf{v}_k$ is measurement error, reflecting the fact that the measurements are not perfect. It is assumed to be uncorrelated white noise with zero mean and covariance $\mathbf{R}$.

The aim of the Kalman filter is to estimate the state, $\mathbf{x}$, from the measurements, $\mathbf{z}$. The basic Kalman filter method processes data sequentially, and consists of 2 steps. The first step is the prediction step, which requires knowledge of the evolution of the state (equation (5.1)). The second step uses data (if available) to improve the estimate of the state, $\mathbf{x}$ and its covariance, $\mathbf{P}$.

Step 1.

$$\tilde{\mathbf{x}}_k = \Phi_{k-1}\hat{\mathbf{x}}_{k-1} + \mathbf{G}_{k-1}\mathbf{u}_{k-1} \tag{5.3}$$

$$\tilde{\mathbf{P}}_k = \Phi_{k-1}\mathbf{P}_{k-1}\Phi_{k-1}^T + \mathbf{Q}_{k-1} \tag{5.4}$$

Step 2.

$$\hat{\mathbf{x}}_k = \tilde{\mathbf{x}}_k + \mathbf{L}_k\left(\mathbf{z}_k - \mathbf{H}_k\tilde{\mathbf{x}}_k\right) \tag{5.5}$$

$$\mathbf{P}_k = (\mathbf{I} - \mathbf{L}_k\mathbf{H}_k)\tilde{\mathbf{P}}_k(\mathbf{I} - \mathbf{L}_k\mathbf{H}_k)^T + \mathbf{L}_k\mathbf{R}_k\mathbf{L}_k^T \tag{5.6}$$

where

$$\mathbf{L}_k = \tilde{\mathbf{P}}_k\mathbf{H}_k^T(\mathbf{H}_k\tilde{\mathbf{P}}_k\mathbf{H}_k^T + \mathbf{R}_k)^{-1} \tag{5.7}$$

$\tilde{\mathbf{x}}_k$ is the projection of the state forward from the previous timestep (with covariance $\tilde{\mathbf{P}}_k$) and $\hat{\mathbf{x}}_k$ is the state estimate updated using measurements (with covariance $\mathbf{P}_k$). $\mathbf{L}_k$ is the

Kalman gain matrix. It specifies how much an observation is allowed to alter the state estimate, and depends on the present uncertainty in the state versus the uncertainty in the observation. The state estimates are *optimal*, in the sense that the state error covariance is minimised, and the Kalman gain matrix is derived to give the optimal solution (Brown, 1983; Gelb, 1974). Equation (5.6) for update of the covariance matrix is valid for any gain, suboptimal or otherwise, while there is a simpler expression

$$\mathbf{P}_k = (\mathbf{I} - \mathbf{L}_k\mathbf{H}_k)\tilde{\mathbf{P}}_k \tag{5.8}$$

which is valid only for the Kalman (optimal) gain. The Kalman filter requires Φ, $\mathbf{H}$, $\mathbf{u}$, $\mathbf{Q}$ and $\mathbf{R}$ to be known. These quantities can all vary with time. The initial state and covariance are also required. The above equations describe the linear model; the nonlinear case will be discussed later.

The Kalman filter can be considered to be a form of Bayesian estimation, as at each timestep the prediction from the previous timestep provides a prior estimate. This is then improved using data (Young, 1984). The quantity $\mathbf{z}_k - \mathbf{H}_k\tilde{\mathbf{x}}_k$ is often called the *innovation* or mismatch. Note that this is different to the *residual*, which is given by $\mathbf{z}_k - \mathbf{H}_k\hat{\mathbf{x}}_k$ i.e. using the state as estimated after the update step (Kailath, 1974). The innovation covariance is given by

$$\Gamma_k = \mathbf{H}_k\tilde{\mathbf{P}}_k\mathbf{H}_k^T + \mathbf{R}_k \tag{5.9}$$

The Kalman filter, and its use in trace gas studies, is probably best illustrated by discussion of a simple example. A minimal model for methane can be constructed with just a source term and a single lifetime describing the sink of methane due to destruction by reaction with OH (and other less important sinks). For this simplest case, the state consists of 2 components: concentration (in Tg) and source (in Tg/yr),

$$\mathbf{x} = \begin{bmatrix} \mathrm{CH_4} \\ \mathrm{src} \end{bmatrix} \tag{5.10}$$

The evolution matrix, Φ, describing how the state changes from one timestep to the next is

$$\Phi = \begin{bmatrix} e^{-\delta t/\tau} & \delta t e^{-\delta t/2\tau} \\ 0 & 1 \end{bmatrix} \tag{5.11}$$

The term $\Phi_{11} = e^{-\delta t/\tau}$, where τ is the lifetime of CH_4 in the atmosphere, represents the decay of CH_4 due to destruction. $\Phi_{12} = \delta t e^{-\delta t/2\tau}$ is the effect of the source on atmospheric concentration, and would be equal to δt except that the amount of methane put into the atmosphere from the source over the time interval δt has decayed (on average) for half the time interval δt. The deterministic forcing term, $\mathbf{u}_k$, is the known forcing for the state, for example if the fossil fuel source of methane to the atmosphere was known it could be included here.

A random walk model (Mulquiney et al., 1995) is assumed for evolution of the source in the ice core applications. The random walk model is very simple, assuming persistence plus a random change with some specified variance. It is implemented in the Kalman filter by having $\Phi_{22} = 1.0$ in the evolution matrix and a component of stochastic forcing for the source. The modelled concentration has no stochastic component, its variation being due only to the source and decay. The covariance of stochastic forcing, $\mathbf{Q}$, is then

$$\mathbf{Q} = \begin{bmatrix} 0 & 0 \\ 0 & {q_{\text{src}}}^2 \end{bmatrix} \tag{5.12}$$

where q_{src} controls how much the source can vary from one timestep to the next in the random walk model, and will be discussed in some detail later. $\mathbf{Q}$ is sometimes referred to as the covariance of the model error, as $\mathbf{w}$ represents the inability of the deterministic part of the evolution model to fully describe variations in the state. The error statistics ($\mathbf{Q}$ and $\mathbf{R}$) are very important in these calculations, because the source estimates and their uncertainties depend strongly on the underlying statistical model.

For methane observations in ppb and state variables as defined above, the projection matrix is

$$\mathbf{H} = \begin{bmatrix} \text{ppb/Tg} & 0 \end{bmatrix} \tag{5.13}$$

where ppb/Tg is a unit conversion from Tg CH_4 to ppb (0.3533 ppb/Tg). For times without data, $\mathbf{H} = [0 \quad 0]$. The method is applied to CH_4 data from Law Dome (Etheridge et al., 1998) where uncertainties are estimated to be 5 ppb, so $\mathbf{R} = \begin{bmatrix} 5^2 \end{bmatrix}$. The Law Dome measurements are averaged where there are multiple concentrations in one year to give a single value. They are shifted so that they represent global mean rather than southern hemisphere levels, using the global mean CH_4 estimated by Etheridge et al. (1998) from

Greenland and Law Dome measurements. The lifetime of CH_4 in the atmosphere used in the calculations is that used by Etheridge et al. (1998), 8.1 y for the pre-industrial with a linear increase from 8.1 y in 1800 to 9 y in 1996. The CH_4 lifetime is believed to have increased due to a decrease in global mean OH concentration caused by increases in tropospheric O_3, NO_x, CO and hydrocarbons (Wang and Jacob, 1998). Figures 5.1a and 5.1b show estimates of the state variables (concentration is shown in ppb rather than Tg for comparison with the observations). A time step of 1 year is used and the model often evolves for a number of time steps in a row without comparison with new data. The step form of the curves and saw-tooth-like structure of the uncertainties show how the state and covariance evolve by the evolution equation until a new observation becomes available. The state is then 'corrected' to give a better fit to the observation, with the size of the correction depending on the mismatch, and on the uncertainty in both the predicted state at the current time and the observation. The state uncertainty is lowest immediately after an observation has been used to refine the estimate.

5.2.2 Smoothing

An important improvement to the Kalman filter comes from considering a further step – fixed interval smoothing. In the Kalman filter, at each time, t, the estimate of the state (and covariance) uses only data up to the current time, t_k. (This is denoted by $\mathbf{x}_{k|k}$ and $\mathbf{P}_{k|k}$ in the conventional notation of $\mathbf{x}_{a|b}$ representing the estimate of the state at time t_a using data up to time t_b). In fixed interval smoothing, a second pass is performed over the interval [0,N] so that the estimates at each time depend on all of the data in the interval (i.e. giving $\mathbf{x}_{k|N}$, $\mathbf{P}_{k|N}$). Gelb (1974) introduces the smoother as a linear combination of the forward filter, $\hat{\mathbf{x}}_k$, with covariance $\mathbf{P}_k$ that uses data before time t_k, and a backward filter, $\hat{\mathbf{x}}_k^b$ with covariance $\mathbf{P}_k^b$ that uses only data after t_k (Fraser and Potter, 1969). This optimal smoother is given by

$$\mathbf{x}_{k|N} = \mathbf{P}_{k|N}[{\mathbf{P}_k}^{-1}\hat{\mathbf{x}}_k + {\mathbf{P}_k^b}^{-1}\hat{\mathbf{x}}_k^b] \tag{5.14}$$

$$\mathbf{P}_{k|N} = ({\mathbf{P}_k}^{-1} + {\mathbf{P}_k^b}^{-1})^{-1} \tag{5.15}$$

where $\mathbf{x}_k^b$ and $\mathbf{P}_k^b$ come from running the filter backwards in time from t_N to t_0. This is often referred to as the 2-filter form of the smoother.

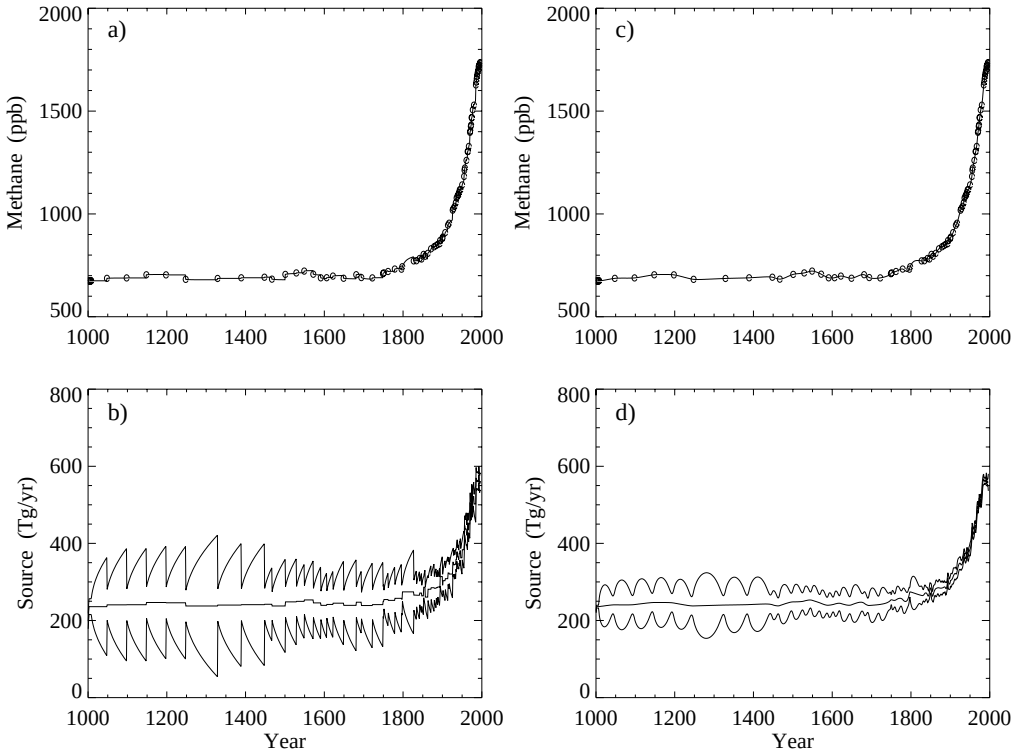

Figure 5.1: Methane concentration and source over the last 1000 years determined with the Kalman filter. a) Methane concentration, where the symbols are Law Dome ice core measurements (Etheridge et al., 1998) and the solid line is the projection of the concentration state variable from the forward pass. b) Estimated source with uncertainty estimates from the forward pass of the Kalman filter. c) Methane concentration from the smoother pass of the Kalman filter with the ice core measurements. d) Source estimates and uncertainties from the Kalman smoother.

There are other computational forms of the smoother equations. A method known as the RTS smoother was developed by Rauch, Tung and Striebel (1965) and is given in Gelb (1974). It also requires a backward pass over the interval [0,N], but differs from the two-pass filter in that the backward pass does not involve processing of the observations. The equations for the RTS smoother are

$$\hat{\mathbf{x}}_{k|N} = \hat{\mathbf{x}}_k + \mathbf{A}_k[\hat{\mathbf{x}}_{k+1|N} - \tilde{\mathbf{x}}_{k+1}] \tag{5.16}$$

$$\mathbf{P}_{k|N} = \mathbf{P}_k + \mathbf{A}_k[\mathbf{P}_{k+1|N} - \tilde{\mathbf{P}}_{k+1}]\mathbf{A}_k^T \tag{5.17}$$

where

$$\mathbf{A}_k = \mathbf{P}_k \Phi_k^T \tilde{\mathbf{P}}_{k+1}^{-1} \tag{5.18}$$

$$\hat{\mathbf{x}}_{N|N} = \hat{\mathbf{x}}_N \tag{5.19}$$

$$\mathbf{P}_{N|N} = \mathbf{P}_N \tag{5.20}$$

In both the 2-filter and RTS smoother methods, the covariance matrix needs to be inverted on the backward pass. In some cases, including the CO_2 and $\delta^{13}C$ application to be considered here, this can be a problem. Bryson and Frazier (1962) gave a third method for smoothing (often referred to as the Bryson-Frazier smoother) which does not require inversion of the covariance matrix. They were in fact the first to present a method for fixed-interval smoothing. Bryson and Frazier formulated the problem for the continuous case as a two point boundary value problem using calculus of variations. Cox (1964) gave the discrete analogue. Derivation of the Bryson-Frazier smoother equations for the discrete case, and how they relate to the RTS smoother, was also given by Bryson and Ho (1975), and is briefly described here.

The problem of smoothing for a single timestep over the time interval $[t_0, t_1]$ is formulated as one of minimising the quadratic

$$\begin{aligned} J = \frac{1}{2}(\mathbf{x}_0 - \hat{\mathbf{x}}_0)^T \mathbf{P}_0^{-1}(\mathbf{x}_0 - \hat{\mathbf{x}}_0) + \frac{1}{2}(\mathbf{w}_0 - \bar{\mathbf{w}}_0)^T \mathbf{Q}_0^{-1}(\mathbf{w}_0 - \bar{\mathbf{w}}_0) \\ + \frac{1}{2}(\mathbf{z}_1 - \mathbf{H}_1\mathbf{x}_1)^T \mathbf{R}_1^{-1}(\mathbf{z}_1 - \mathbf{H}_1\mathbf{x}_1) \end{aligned} \tag{5.21}$$

subject to the constraint

$$\mathbf{x}_1 = \Phi_0 \mathbf{x}_0 + \mathbf{w}_0 \tag{5.22}$$

The form of equation (5.21) is quite common, and gives the weighted-least-squares estimate of the state, x, taking into account the statistics of the stochastic forcing, w and the measurement, z. The weighting matrices are the inverse covariance matrices, i.e. $\mathbf{P}^{-1}$, $\mathbf{Q}^{-1}$ and $\mathbf{R}^{-1}$. The minimum for J is found by writing equations (5.21) and (5.22) in terms of differential changes, eliminating dx_1 and setting $dJ = 0$. After manipulations using the forward filter equations, $\mathbf{x}_{0|1}$ and $\mathbf{P}_{0|1}$ can be written as

$$\hat{\mathbf{x}}_{0|1} = \hat{\mathbf{x}}_0 - \mathbf{P}_0 \Phi_0^T \tilde{\mathbf{P}}_1^{-1}(\tilde{\mathbf{x}}_1 - \hat{\mathbf{x}}_1) \tag{5.23}$$

$$\mathbf{P}_{0|1} = \mathbf{P}_0 - \mathbf{P}_0 \Phi_0^T \tilde{\mathbf{P}}_1^{-1} (\tilde{\mathbf{P}}_1 - \mathbf{P}_1)[\mathbf{P}_0 \Phi_0^T \tilde{\mathbf{P}}_1^{-1}]^T \tag{5.24}$$

which are the RTS equations.

By defining λ_0 and Λ_0 as

$$\lambda_0 \equiv \tilde{\mathbf{P}}_1^{-1}(\tilde{\mathbf{x}}_1 - \hat{\mathbf{x}}_1) = -\mathbf{H}_1^T (\mathbf{H}_1^T \tilde{\mathbf{P}}_1 \mathbf{H}_1 + \mathbf{R}_1)^{-1} (\mathbf{z}_1 - \mathbf{H}_1 \tilde{\mathbf{x}}_1) \tag{5.25}$$

$$\Lambda_0 \equiv \tilde{\mathbf{P}}_1^{-1}(\tilde{\mathbf{P}}_1 - \mathbf{P}_1) = \mathbf{H}_1^T (\mathbf{H}_1 \tilde{\mathbf{P}}_1 \mathbf{H}_1^T + \mathbf{R}_1)^{-1} \mathbf{H}_1 \tag{5.26}$$

which use the Kalman filter equations ((5.5), (5.7) and (5.8)), equations (5.23) and (5.24) can be written as

$$\hat{\mathbf{x}}_{0|1} = \hat{\mathbf{x}}_0 - \mathbf{P}_0 \Phi_0^T \lambda_0 \tag{5.27}$$

$$\mathbf{P}_{0|1} = \mathbf{P}_0 - \mathbf{P}_0 \Phi_0^T \Lambda_0 \Phi_0 \mathbf{P}_0 \tag{5.28}$$

λ and Λ have the same dimensions as the state vector and state covariance, respectively. Sequential application of these equations backwards in time gives the smoother for multiple timesteps. A forward sweep using the observations is needed to estimate $\hat{\mathbf{x}}_k$ and $\mathbf{P}_k$. Then, with $\hat{\mathbf{x}}_{N|N} = \hat{\mathbf{x}}_N$ and $\hat{\mathbf{P}}_{N|N} = \hat{\mathbf{P}}_N$ the following equations are solved recursively for the smoother solution

$$\hat{\mathbf{x}}_{k|N} = \hat{\mathbf{x}}_k - \mathbf{P}_k \Phi_k^T \lambda_k \tag{5.29}$$

$$\lambda_{k-1} = (\mathbf{I} - \mathbf{P}_k \mathbf{S}_k)^T [\Phi_k^T \lambda_k - \mathbf{H}_k^T \mathbf{R}_k^{-1} (\mathbf{z}_k - \mathbf{H}_k \tilde{\mathbf{x}}_k)], \qquad \lambda_N = 0 \tag{5.30}$$

$$\mathbf{P}_{k|N} = \mathbf{P}_k - \mathbf{P}_k \Phi_k^T \Lambda_k \Phi_k \mathbf{P}_k \tag{5.31}$$

$$\Lambda_{k-1} = (\mathbf{I} - \mathbf{P}_k \mathbf{S}_k)^T \Phi_k^T \Lambda_k \Phi_k (\mathbf{I} - \mathbf{P}_k \mathbf{S}_k) + \mathbf{S}_k (\mathbf{I} - \mathbf{P}_k \mathbf{S}_k), \qquad \Lambda_N = 0 \tag{5.32}$$

where

$$\mathbf{S}_k = \mathbf{H}_k^T \mathbf{R}_k^{-1} \mathbf{H}_k \tag{5.33}$$

Although the Bryson-Frazier smoother has the advantage of avoiding matrix inversion, a disadvantage of the method is that it involves taking differences of matrices that may be large (Bryson and Ho, 1975).

λ is an auxiliary variable for the calculation. The smoother avoids inverting the covariance matrix by instead propagating λ backwards in time, where λ has the following mathematical interpretation

$$\lambda_k = \mathbf{P}_{k+1|k}^{-1}(\hat{\mathbf{x}}_{k+1|N} - \hat{\mathbf{x}}_{k+1|k}) \tag{5.34}$$

(Meditch, 1973). This smoother has some similarities to the adjoint method, which also propagates information backwards in time. The physics of the adjoint model are represented by Φ^T (Wunsch, 1996, p130; Errico, 1997), and give the sensitivity of model output to input (e.g. sensitivity of concentrations to sources for the trace gas problem (Kaminski et al., 1999)). In fact, the Kalman filter/smoother and the adjoint method produce identical results for linear models (Wunsch, 1996, p380).

When the value of a constant is estimated with the Kalman filter and smoother, (i.e. where the evolution of a state variable has only a 1.0 on the diagonal and the relevant term in $\mathbf{Q}$ is zero), the smoother doesn't change the value from the filter estimate at the final time, as the filter has already used all data (i.e. $\hat{\mathbf{x}}_{k|N} = \hat{\mathbf{x}}_{N|N}$). Such models are termed 'non-smoothable'.

Figures 5.1c and 5.1d show estimates from the smoother pass for the methane ice core case. The step-like structure of the forward pass is no longer apparent, and estimates of the time variation of the sources look more realistic. The uncertainty on the source estimate is greatest midway between data points, as would be expected.

5.2.3 Extended Kalman filter

The Kalman filter and smoother equations given above apply for linear models, but the equations that will be developed for CO_2 and $\delta^{13}C$ are nonlinear. The Extended Kalman filter (Young, 1984, Sec. 9.2; Gelb, 1974, Sec. 6.1; Jazwinski, 1970, Sec. 8.3) is an algorithm for nonlinear systems that is developed by linearising the model equations and is very similar in application to the linear Kalman filter. The nonlinear model is defined by

$$\frac{d\mathbf{x}_k}{dt} = \mathbf{f}(\mathbf{x}_k, \mathbf{u}_k, k) + \mathbf{w}_k \tag{5.35}$$

$$\mathbf{z}_k = \mathbf{h}(\mathbf{x}_k, k) + \mathbf{v}_k \tag{5.36}$$

where $\mathbf{f}$ and $\mathbf{h}$ are known functions. For n state variables and m observations, $\mathbf{f}$ has n equations, each one giving the evolution equation of one state variable as a function of

all state variables, and $\mathbf{h}$ has m equations, each one giving the projection of all state variables onto each observation. The Extended Kalman filter is derived by linearising equations (5.35) and (5.36) about the calculated Kalman filter trajectory, i.e. the current state estimate at each time. The state is propagated in time using the nonlinear equation (5.35), and the innovations in equation (5.5) are calculated by $\nu_k = \mathbf{z}_k - \mathbf{h}(\mathbf{x}_k, k)$. Partial derivative matrices (Jacobians) are constructed to give the following evolution and projection matrices

$$\Phi = \begin{bmatrix} \frac{\partial \mathrm{f}_1}{\partial \mathrm{x}_1} & \frac{\partial \mathrm{f}_1}{\partial \mathrm{x}_2} & . & . & . \\ \frac{\partial \mathrm{f}_2}{\partial \mathrm{x}_1} & \frac{\partial \mathrm{f}_2}{\partial \mathrm{x}_2} & . & . & . \\ . & & & & \\ . & & & & \\ . & & & & \end{bmatrix} \qquad \mathbf{H} = \begin{bmatrix} \frac{\partial \mathrm{h}_1}{\partial \mathrm{x}_1} & \frac{\partial \mathrm{h}_1}{\partial \mathrm{x}_2} & . & . & . \\ \frac{\partial \mathrm{h}_2}{\partial \mathrm{x}_1} & \frac{\partial \mathrm{h}_2}{\partial \mathrm{x}_2} & . & . & . \\ . & & & & \\ . & & & & \\ . & & & & \end{bmatrix} \tag{5.37}$$

where $\partial \mathrm{f}_i / \partial \mathrm{x}_j$ is the derivative of the evolution equation for x_i with respect to x_j and $\partial \mathrm{h}_i / \partial \mathrm{x}_j$ the derivative of the projection equation for observation i with respect to x_j. These matrices are used in the linear Kalman filter equations ((5.4), (5.6) and (5.7)) and change with time as the state changes. The covariance of the deviation of the state from a reference trajectory is approximately equal to the covariance of the state, provided the state deviations are small (Jazwinski, 1970). The Linearised Kalman filter is essentially the same as the Extended Kalman filter, except that the linearisation is about a pre-computed trajectory. It would depend on the application whether the Linearised or Extended Kalman filter would be best suited.

The smoother equations described in the previous section were all for the linear case. Extension of these smoothers to the nonlinear case needs to be addressed for the nonlinear CO_2 and $\delta^{13}C$ case. Gelb (1974) describes application of the two-filter and RTS smoothers to nonlinear problems. Cox (1964) gave a linearised version of the Bryson-Frazier smoother equations that closely resemble the equations for the linear case. The linearised Bryson-Frazier smoother involves solving the same equations as for the linear case, but with Φ and $\mathbf{H}$ given by equation (5.37) and with equation (5.30) replaced by

$$\lambda_{k-1} = (\mathbf{I} - \mathbf{P}_k \mathbf{S}_k)^T [\Phi_k^T \lambda_k - \mathbf{H}_k^T \mathbf{R}_k^{-1} (\mathbf{z}_k - \mathbf{h}(\tilde{\mathbf{x}}_k, k))]. \tag{5.38}$$

This method will be used for the nonlinear CO_2 and $\delta^{13}C$ calculation.

There are many more variations to the Kalman filter than those mentioned here, and the best one for a particular application will depend on its constraints. For example, some applications are run in real-time, so that each state estimate is calculated before observations at later times become available. In the case of ice core analysis, all of the observations are available before processing begins, so it makes sense to use all observations for state estimates at all times via the smoothing techniques. Other applications are run in 'real time', such as controlling the flight of an aeroplane, where fast, efficient algorithms are essential. Fast processing is not a particular requirement for the analysis of the ice core data.

5.3 Previous applications of Kalman filtering to trace gas studies

The Kalman filter has been applied to a wide range of problems in science and engineering, including some applications to trace gas studies. Surendran and Mulholland (1986; 1987) analysed variations in the Mauna Loa CO_2 record using the Kalman filter. In Surendran and Mulholland (1986) they modelled concentrations as an exponential increase with a sinusoidal oscillation for the annual cycle, and tried to estimate atmospheric CO_2 concentration and the airborne fraction. They used adaptive filtering (adaptive filtering involves using the statistics of the innovations to test for optimality and estimate $\mathbf{Q}$ and $\mathbf{R}$ if these are unknown; see Section 5.4) to estimate $\mathbf{Q}$, where the stochastic noise term represented inaccuracies in modelling Mauna Loa CO_2 by the evolution equation. Surendran and Mulholland (1987) used adaptive filtering to estimate the precision and accuracy of CO_2 measurements (i.e. they estimated the measurement noise covariance, $\mathbf{R}$), where CO_2 variation was modelled as an exponential increase with periodic components for the seasonal cycle and an autoregressive model of order 2 for quasiperiodic behaviour. Enting (1989a) also modelled Mauna Loa CO_2, with two different models (a constant airborne fraction and a mean lifetime for fossil CO_2), but without a stochastic forcing component (i.e. $\mathbf{Q} = 0$).

Enting (1989b) applied the Kalman filter to the deconvolution of CO_2 since 1800 using measurements from Mauna Loa and the Siple ice core record. Ocean uptake was modelled in terms of a response function with a single lifetime, and the net biotic flux was estimated

from the CO_2 data. The state had 2 components – the biotic flux and the perturbation to CO_2 concentration from pre-industrial levels. $\mathbf{w}_k$ acted as the stochastic forcing for the biospheric flux, giving a random walk model for flux evolution as in the methane example already described. The Kalman filtering analysis of ice core measurements in this chapter builds on this work by Enting (1989b).

Mulquiney et al. (1995) investigated the use of the Kalman filter with a random walk model for deducing fluxes of greenhouse gases with flux evolution modelled as

$$\mathbf{x}_k = \mathbf{x}_{k-1} + \mathbf{w}_k \tag{5.39}$$

They concluded that the random walk model is able to handle typical features of actual flux evolution, and that used with the Kalman filter had reasonable prospect of success, as long as the dynamical relation between fluxes and measured concentrations could be adequately modelled.

The Kalman filter has been used in a number of studies to predict the atmospheric lifetime or sources of CFCs. One such early study was Cunnold et al. (1983). More recently, Hartley and Prinn (1993) looked at using the Kalman filter to deduce the spatial distribution of sources from concentration measurements. They used CFC-11 ($CFCl_3$) because the sources are relatively well known. Their state vector contained emissions from 5 source regions, and they used observations of concentrations at 5 sampling sites. A 3-d chemical transport model was used to relate concentrations and emissions. Their method consisted of running the transport model for one month with the current source estimate, comparing calculated concentrations with observations, and updating the emissions using the mismatch in concentrations in the Kalman filter equations. Rather than putting the full 3-d model equations into the Kalman filter, a Jacobian (a partial derivative matrix, containing the response at each observation site to the source in each source region) was generated by the 3-d model and used in the Kalman filter. This is, in effect, how the Extended Kalman filter is implemented. The calculation was first run with pseudo-data (model generated data, so that it could be assumed that the transport was perfectly represented by the transport model), then with real data. They had no stochastic forcing term, i.e. $\mathbf{Q} = 0$, so the method estimated constant sources.

Haas-Laursen et al. (1996) extended the work of Hartley and Prinn (1993) to test deduction of time-varying sources. They had no stochastic forcing, but used an adaptive

filter, where the covariance matrix was reset to its initial value when the calculated mixing ratio began to diverge from the observations. They also used an adaptive-iterative method, where the adaptive filtering method was iterated until the change in emissions from one timestep to the next was sufficiently small. Mulquiney and Norton (1998) and Mulquiney et al. (1998) also looked at deducing time-varying sources of CFC-11, but used the random walk model for source evolution. Like Hartley and Prinn, they first tested their model on pseudo-data, then applied it to real observations. The values they used in $\mathbf{R}$ were significantly greater than the actual noise in the measurements because they wanted to reduce the variability in the emission estimates. Their $\mathbf{Q}$ had nonzero values for both source and concentration components, with smaller values for the sources than concentrations, again to ensure smoothness of the estimated sources.

As well as global source distributions, the Kalman filter has been applied to deducing regional (limited area) source distributions. Mulholland and Seinfeld (1995) applied the Kalman filter to estimation of carbon monoxide emissions for the Los Angeles Basin. Stijnen et al. (1997) estimated methane emissions over Europe. There are a number of complications associated with atmospheric transport that are important for spatial inversions but are (fortunately) not relevant to the ice core analysis. Examples of these include the time delay for a source component to reach an observation location, and the fact that the concentration is affected by sources on a wide range of spatial and temporal scales.

5.4 Choosing Q for ice core analysis

The Kalman filter results depend quite heavily on the covariance of the stochastic forcing, $\mathbf{Q}$, so the choice of suitable values is very important. The form of $\mathbf{Q}$ has already been defined for the ice core applications to give random walk variation for the source component, however it is not obvious what the magnitude of this variation (specified by the elements of $\mathbf{Q}$) should be. Choice of $\mathbf{Q}$ will be guided by both the physics of the system (using estimates of how much the source varies from year to year, with some account made for the smoothing of the atmospheric record by the firn and ice core processes) and the statistics (by ensuring that the Kalman filter assumptions are satisfied). If $\mathbf{Q}$ is too small then the state variables can't vary enough to adequately match the time variations in the

data, and if it is too big then the state varies too much and the Kalman filter may track noisy data too closely. The measurement noise covariance, $\mathbf{R}$, also specifies how closely the filter fits the observations. The quantity $\mathbf{Q}/\mathbf{R}$ is actually what is important, more than the values of either $\mathbf{Q}$ or $\mathbf{R}$ individually.

It is worth pointing out that, in a way, the interpretation of $\mathbf{Q}$ (and $\mathbf{w}$) used here differs slightly from that in most applications of the Kalman filter. Many applications use $\mathbf{Q}$ for model error, for example in numerical weather prediction the model error is the error in the predicted state due to the model not perfectly representing the real world (Dee, 1995). The interpretation used here is that $\mathbf{Q}$ describes source variability. Whether the interpretation of $\mathbf{Q}$ is source variability or model error, it still describes the inability of the deterministic model to predict into the future. In the source case, we don't even try to model the source variation in the deterministic part of the model. Probably the main difference between the two interpretations is that in the source case we are actually very interested in the variation described by $\mathbf{Q}$, while in most other applications it is treated more as a nuisance, i.e. the prior model is purely 'stochastic', not 'deterministic with stochastic errors'.

The simple CH_4 example shown in Figure 5.1 uses no deterministic forcing, and $q_{\text{src}} = 20$ Tg yr^{-1} in equation (5.12) to give

$$\mathbf{Q} = \begin{bmatrix} 0 & 0 \\ 0 & 400 \end{bmatrix} \tag{5.40}$$

q_{src} needs to account for variation in the source from one timestep to the next. $q_{\text{src}} = 20$ Tg yr^{-1} was chosen to allow the source to change by about 200 Tg over 150 years, by a sequence of 150 independent annual changes of rms value q_{src}, where $q_{\text{src}}\sqrt{150} = 200$, giving a value for q_{src} of around 20 Tg yr^{-1}. This gives quite large uncertainties on the predicted pre-industrial source, because the year-to-year variation required to model the anthropogenic source in the random walk model is much greater than would be expected for natural variation in the sources.

The sequence of innovations ($\nu_k = \mathbf{z}_k - \mathbf{H}_k\tilde{\mathbf{x}}_k$) can tell us a lot about the statistics of the Kalman filter and whether its assumptions are being satisfied. The innovation sequence can also be used to estimate the appropriate $\mathbf{Q}$ and $\mathbf{R}$ using an adaptive Kalman filter (Mehra, 1970). For an optimal filter, the innovation sequence is a realisation of a Gaussian white

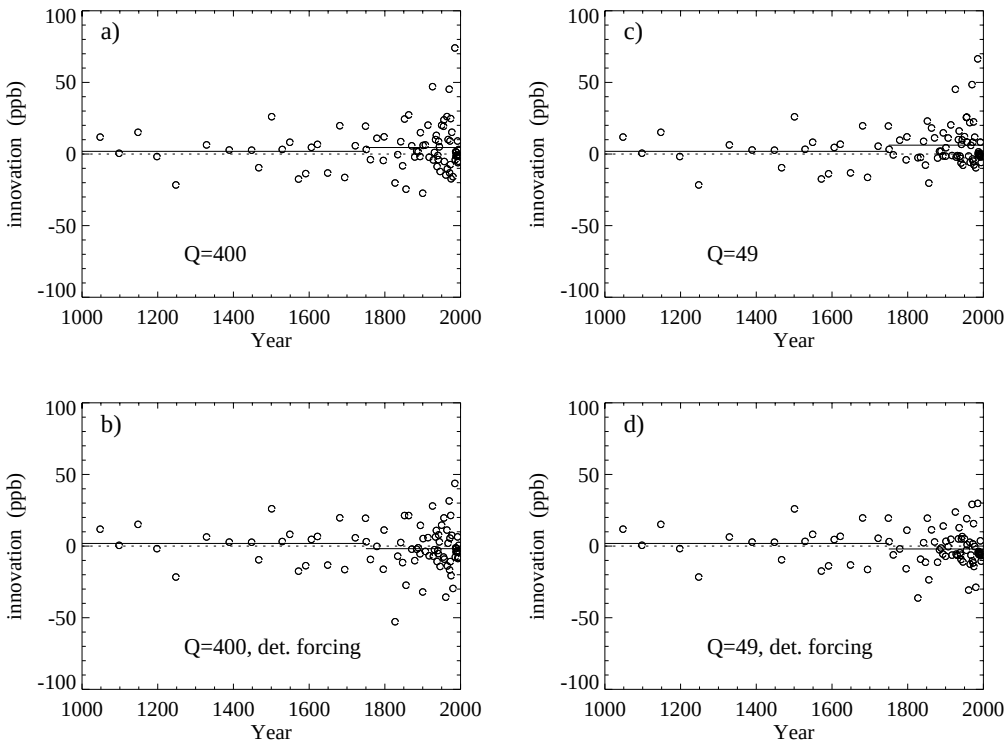

Figure 5.2: Sequence of innovations for the methane calculation. a) $q_{\rm src} = 20$, (corresponding to $\mathbf{Q}$= 400 (Tg yr^{-1})^2), no deterministic forcing, b) $q_{\rm src} = 20$ Tg yr^{-1}, deterministic forcing, c) $q_{\rm src} = 7$ Tg yr^{-1}, no deterministic forcing, d) $q_{\rm src} = 7$ Tg yr^{-1}, deterministic forcing.

noise sequence and therefore has zero mean (Mehra, 1970). The innovation covariance is given by equation (5.9). The optimality of a Kalman filter can be tested using the statistics of the innovations. Figure 5.2a shows the innovations for the CH_4 example with $q_{\rm src} = 20$ Tg yr^{-1}. As the source has quite different characteristics in the pre-industrial and industrial periods, these 2 periods will be considered separately, with the boundary taken to be 1750. The solid lines in Figure 5.2a show the average of the innovations for the two periods. The mean for the pre-industrial is close to zero. For the industrial period the mean is slightly positive (5.4 ppb) due to the continually increasing source.

The Kalman filter may perform better if the anthropogenic source of CH_4 is specified as a deterministic forcing. This should reduce the size of the steps needed by the random walk model and therefore reduce the uncertainties on the calculated sources, as well as shifting

the mean of the innovations closer to zero. The deterministic forcing is unfortunately not well known for CH_4, but the general form of the source increase can be seen from the previous calculation. It is due to a number of anthropogenic activities, including rice production, livestock, landfill, biomass burning and coal mining. The methane calculation is repeated with a deterministic source component set proportional to estimated global population, with

$$\mathbf{u}_k = 400 \times \frac{P(t_k) - P(1750)}{P(1990) - P(1750)} \tag{5.41}$$

where the source changes by about 400 Tg yr^{-1} from 1750 to 1990 and $P(t_k)$ is the population at time t_k. A simple curve from Demeny (1990) is used for the population, and the long term increase of the anthropogenic source is actually captured quite well in this way. The innovations for the calculation with the deterministic source proportional to population (and $q_{\text{src}} = 20$ Tg yr^{-1}) are shown in Figure 5.2b. The innovation mean for the industrial period is closer to zero (-0.9 ppb) with the deterministic forcing than without, although for this value of q_{src} the model is alright without deterministic forcing.

Another important test of the Kalman filter can be performed by looking at the covariance of the innovations. One way to test this is using the χ^2 (chi-squared) test, where

$$\chi_k^2 = (\mathbf{z}_k - \mathbf{H}_k\tilde{\mathbf{x}}_k)^T \left(\mathbf{H}_k\tilde{\mathbf{P}}_k\mathbf{H}_k^T + \mathbf{R}_k\right)^{-1} (\mathbf{z}_k - \mathbf{H}_k\tilde{\mathbf{x}}_k) \tag{5.42a}$$

$$= \nu_k^T \Gamma_k^{-1} \nu_k \tag{5.42b}$$

is calculated for each observation. The calculated χ^2 is compared with the χ^2 statistical distribution to see whether the measured ($\mathbf{z}_k$) and predicted ($\mathbf{H}_k\tilde{\mathbf{x}}_k$) concentrations have the same statistical distributions. With one degree of freedom, the mean of the calculated χ^2 should be 1 (Tarantola, 1987, p211), although as there are only a relatively small number of observations, the mean is not expected to be exactly 1. Figure 5.3 shows χ^2 for the CH_4 calculation with deterministic forcing and 4 different values of q_{src}. With $q_{\text{src}} = 7$ Tg yr^{-1} the mean χ^2 is very close to 1 for the industrial period. Figure 5.2c and 5.2d show the innovations for $q_{\text{src}} = 7$ Tg yr^{-1} with and without deterministic forcing. The innovation mean is further from zero (7.3 ppb) with this value of q_{src} and no deterministic forcing than in the original calculation. Based on the means of χ^2 and the innovations, $q_{\text{src}} = 7$ Tg yr^{-1} is chosen for the methane calculation over the industrial period. Further analysis should

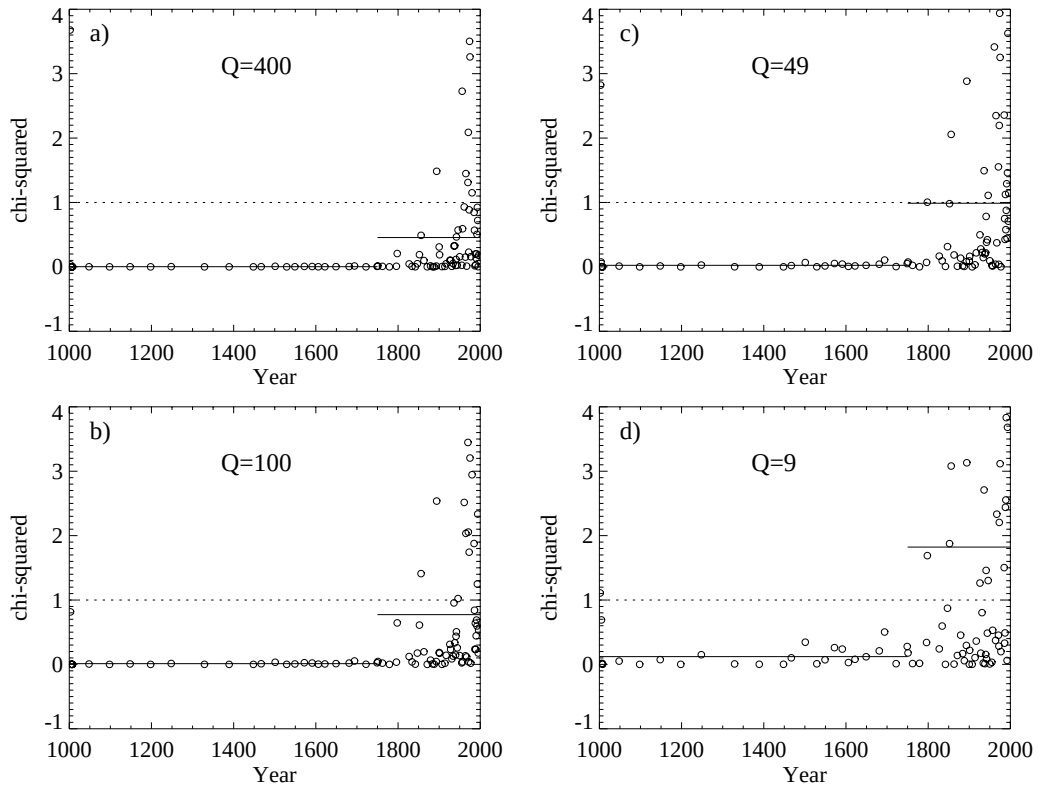

Figure 5.3: Sequence of chi-squared for the methane calculation for different values of **Q**. A deterministic input proportional to population is used in these calculations.

be done to ensure that the value of **Q** suggested by the statistics is physically reasonable. This will not be done for methane, but will be investigated in detail for CO_2 and $\delta^{13}C$.

The value of χ^2 at different times through a calculation can hold information about different aspects of the Kalman filter. According to R. Ménard (pers. comm., 1998), if χ^2 is far from 1 initially, then the initial state covariance is probably wrong. If χ^2 is translated relative to 1 then the data error (**R**) is probably wrong and if χ^2 varies linearly with time then the model error (**Q**) is probably wrong. This type of analysis of χ^2 is useful for applications with a large number of observations at each timestep. The CH_4 ice core example is quite different, having only 84 measurements spread over 1000 years. A translation in χ^2 has been interpreted here in terms of **Q**, rather than **R** as suggested by R. Ménard (pers. comm., 1998). For trace gas studies it is often fairly easy to estimate the uncertainty in the concentration measurement, and it is the ratio of **Q** to **R** that controls the smoothing in the Kalman filter, more than either **Q** or **R** on their own.

There are other ways of testing the innovations that are essentially equivalent to the χ^2 test. For example, the 'Jazwinski filter' (Jazwinski, 1969; 1970) is an adaptive filter that estimates $\mathbf{Q}$ as the calculation proceeds using feedback from the innovations. With $\mathbf{Q}_k = q_k \mathbf{I}$, q_k is estimated by

$$\hat{q}_k = \begin{cases} \frac{\nu_{k+1}^2 - (\mathbf{H}\tilde{\mathbf{P}}\mathbf{H}^T + \mathbf{R})}{\mathbf{H}\mathbf{H}^T} & \text{if positive} \\ 0 & \text{otherwise} \end{cases} \tag{5.43}$$

Comparison of $\nu^2 - (\mathbf{H}\tilde{\mathbf{P}}\mathbf{H}^T + \mathbf{R})$ with zero is equivalent to comparing χ^2 to 1 in the chi-squared test. When this quantity is negative, the innovations are within their standard deviation and the filter is acceptable. When it is positive, the filter is diverging and the state covariance needs to be increased (via $\mathbf{Q}$) so that it is open to new observations. Estimation of $\mathbf{Q}$ with equation (5.43) requires a large number of observations at each timestep for good statistics, and is therefore not suitable for the ice core application. The adaptive filter used by Haas-Laursen et al. (1996) to deduce CFC-11 sources operates in a roughly similar way to the Jazwinski filter. They reset the covariance to its initial value when an inconsistency is detected, rather than estimating the $\mathbf{Q}$ that needs to be added to the covariance. The random walk model for source variation with χ^2 used to help choose $\mathbf{Q}$, as described above, seems like a better approach for source deduction problems than the adaptive filtering method for tracers like CH_4 or CO_2 whose sources are continually varying due to anthropogenic inputs and climate variation.

Choice of $\mathbf{Q}$ requires consideration of the source variation for the *relevant* time scale (e.g. annual, decadal or century). An important aspect of the ice core data is that there are large gaps in the record. Taking account of the smoothing due to firn processes, the ice core measurements would be capable of giving information about the source on decadal time scales if they were sampled regularly enough throughout the record. However, with a data density of roughly one observation every 50 years through the pre-industrial period, decadal variations are obviously not resolvable. The best that can be hoped for is to resolve century time scale source variations. χ^2 over the pre-industrial period has values that are much closer to zero than 1 for the values of $\mathbf{Q}$ shown in Figure 5.3. In the forward pass of the Kalman filter, the source uncertainty at the end of a large data gap is large, and the observation uncertainty small, so it is easy for the Kalman filter to fit the model to the observation, and χ^2 is consequently small. For $q_{\text{src}} = 1$ Tg yr^{-1}, the mean χ^2 for the pre-

industrial is 0.72 and the uncertainty on the source is fairly small. The reduced uncertainty reflects the fact that century time scale variations can be determined more accurately than decadal variations with this data density (see Figure 5.4 in the next section). Knowledge of the amount of variation that occurs in the source on annual, decadal and century time scales is very important. Between 1000 and 1700 AD, the methane source varies by only a small amount away from equilibrium, and the annual, decadal and century variations are probably fairly similar. In a sense, the value of **Q** chooses the time scale that will be resolved by the model. A small **Q** won't allow the model source to vary enough to give the short time scale variations. For example, $q_{\mathrm{src}} = 1$ Tg yr^{-1} would allow the source to vary on the order of 10 Tg yr^{-1} over 100 years, but only around 3 Tg yr^{-1} in 10 years. The uncertainties on the fluxes are smaller for longer time scales.

The methane model described here, with a single source component, tries to model source variation on a range of time scales with a single value of **Q**. Other variations for the source model are possible. For example, the source could be split into 2 components (state variables), with one slowly-varying source component that can be estimated quite accurately (say, century time scale variations), and a rapidly-varying component that is not resolvable and is treated as a nuisance variable (e.g. decadal variations, which are not resolvable in the pre-industrial period due to the low data density). Each source component could have a different **Q**, and different values in the evolution matrix (the rapidly varying component might have a value less than 1.0 in the evolution matrix, so variations in this component decay away between data points). This, or any other source model configuration, should be tested by considering the innovations and the physics.

5.5 Discussion of methane results

Etheridge et al. (1998) gave a detailed discussion of the interpretation of the Law Dome methane ice core record. Only a very brief discussion of the modelling results is given here, as the main focus is on CO_2 rather than CH_4. Methane has been used to demonstrate use of the Kalman filter for interpreting ice core measurements, and in particular the importance of **Q**.

The calculation assumes that the atmospheric lifetime of methane varies as described in Section 5.2.1. Estimates of the lifetime vary quite considerably, and Etheridge et al.

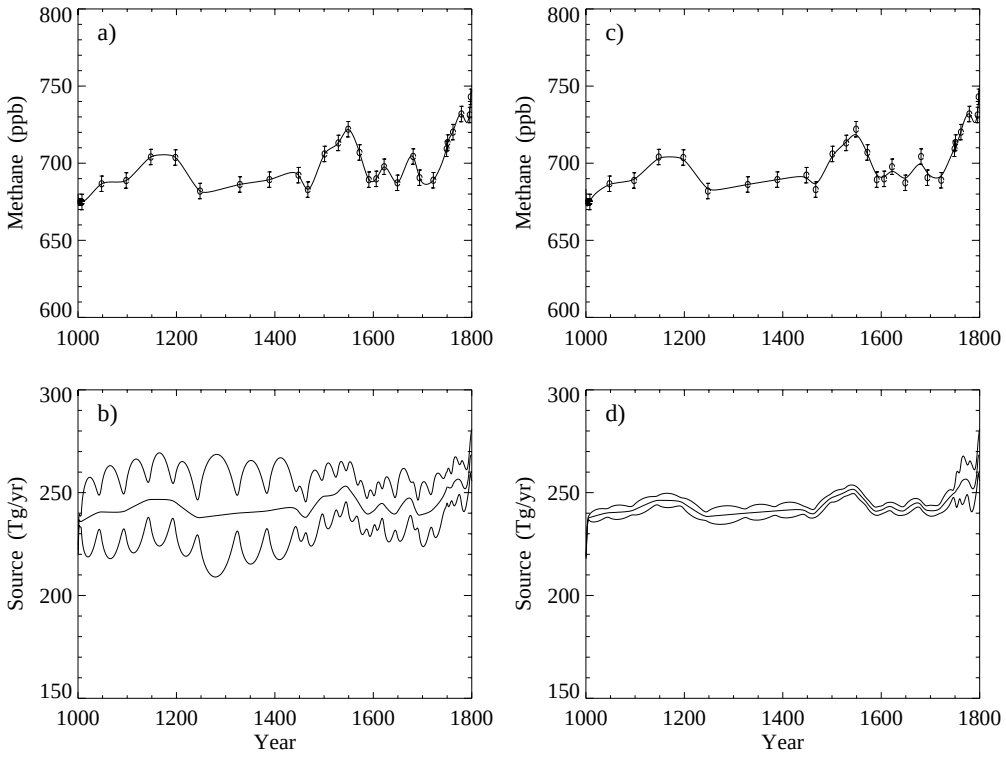

Figure 5.4: Methane concentration and source over the pre-industrial from the Kalman filter for a) and b) $q_{\rm src} = 7$ Tg yr^{-1} and c) and d) $q_{\rm src} = 1$ Tg yr^{-1}. Uncertainties on the source estimates and concentration measurements are shown.

(1998) show the sensitivity of the calculated source to assumed lifetime. The calculated methane source also includes a soil sink of perhaps 10 Tg yr^{-1} (Etheridge et al., 1998). Figure 5.4 shows the calculated methane concentration and source between 1000 and 1800 for $q_{\rm src} = 7$ Tg yr^{-1} and $q_{\rm src} = 1$ Tg yr^{-1}. Uncertainties are plotted for the concentration measurements. The source is low during the Little Ice Age, roughly 1550–1750, as well as between about 1250–1450. The two calculations have very similar variations on century-time scales, but the $q_{\rm src} = 1$ Tg yr^{-1} case smoothes more than the $q_{\rm src} = 7$ Tg yr^{-1} case, and has smaller source uncertainties.

Figure 5.5 shows the results for 1800-1996. Uncertainties in concentration measurements (5 ppb) are shown, but are smaller than the plotting symbols. Estimates of methane sources are very similar to those calculated by Etheridge et al. (1998) from a spline fit to the measurements, as expected because the same variation in atmospheric lifetime is used. A major feature of CH_4 in recent years has been the decrease in the growth rate of

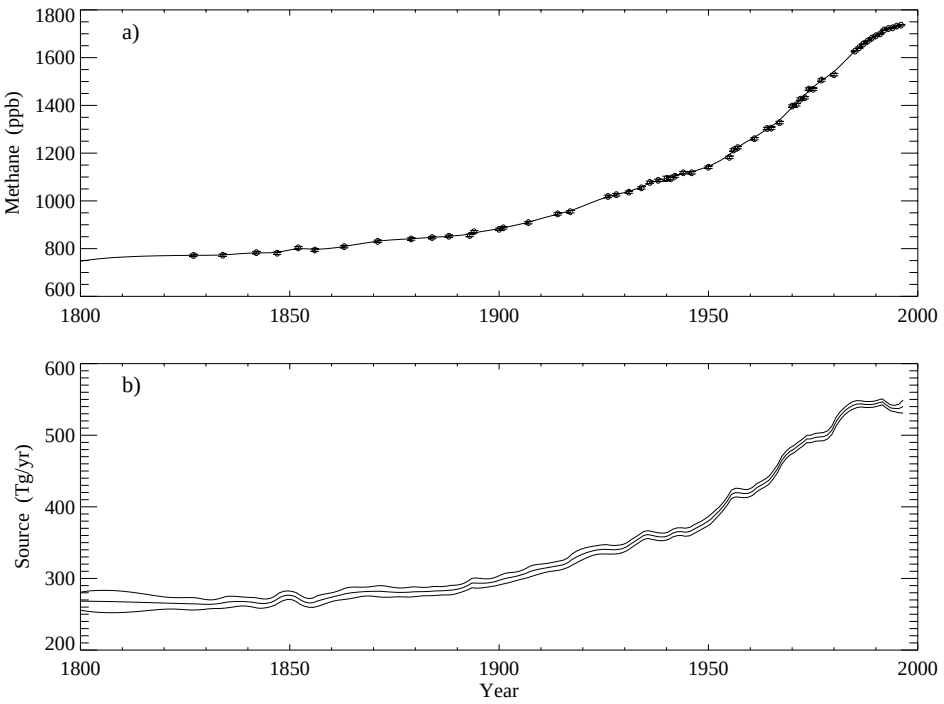

Figure 5.5: Methane concentration and source since 1800 from the Kalman filter. Uncertainties on the concentrations are shown. The calculation uses $q_{\rm src} = 7$ Tg yr^{-1}.

atmospheric concentration (Steele et al., 1992). The source calculated with the Kalman filter is roughly constant from 1985-96, rather than increasing with time as it has done since about 1850. Francey et al. (1999b) used $\delta^{13}CH_4$ since 1978 from the DE08-2 firn and the Cape Grim Air Archive to look at the methane growth rate decrease with a 4 box model. They concluded that both CH_4 and $\delta^{13}CH_4$ are consistent with constant sources since 1978, and that methane is coming to a new equilibrium.

The methane calculations presented here have been valuable for demonstrating and testing application of the Kalman filter technique to ice core records, but they stop short of really adding much to the understanding of the methane budget. Further understanding of methane should come from interpreting the variation of $\delta^{13}CH_4$ and CO as well as CH_4 over this century, for example using measurements from the DSSW20K firn, and perhaps treating the northern and southern hemispheres separately. Based on the results so far, the Kalman filter would probably be a suitable modelling framework to do this, perhaps with both stochastic and deterministic forcing.

5.6 CO_2 and $\delta^{13}C$: atmospheric pulse response functions

5.6.1 Model formulation

Application of Kalman filtering to CO_2 and $\delta^{13}C$ requires equations for the evolution of the state. Taking CO_2 first, uptake by the ocean can be written using a response function, $R(t)$, that is the sum of exponentials (Enting and Mansbridge, 1987; Maier-Reimer and Hasselman, 1987; Enting et al., 1994). For a time-varying source, $S(t)$, that is zero for $t < 0$, the concentration $C(t)$ is given by

$$C(t) = C(0) + \int_0^t R(t - t')S(t')dt' \tag{5.44}$$

where the response function, $R(t-t')$, describes how a pulse of CO_2 is taken up by exchange with the ocean. The BDM (with the parameters calibrated for the single deconvolution in Chapter 4) gives a CO_2 pulse response, shown in Figure 5.6a, that can be written as

$$R(t) = 0.128 + 0.3398e^{-t/2.315} + 0.2372e^{-t/25.23} + 0.295e^{-t/199.4} \tag{5.45}$$

Enting (1989b) applied the Kalman filter to CO_2 using a single exponential. An important advantage of specifying the response function as a sum of exponentials is that the model can be put into a simple autoregressive (AR1) form by considering a number of atmospheric carbon 'pools' with different 'lifetimes' (Wigley, 1991). For $R(t)$ given by equation (5.45), a source of carbon to the atmosphere would be distributed amongst the 4 'pools' using the coefficients 0.1280, 0.3398, 0.2372 and 0.2950, and the pools would have lifetimes of ∞, 2.315, 25.23 and 199.4 years, respectively. For the Kalman filter implementation, the state variables correspond to the amount of carbon in each of the 'pools'.

For extension to $\delta^{13}C$, a simplistic approach of using the BDM to calculate a response function for $\delta^{13}C$ in ‰ due to a pulse of CO_2 will be used. Characterising the behaviour of $\delta^{13}C$ in the atmosphere in this way is certainly not guaranteed to work very well, particularly because atmospheric $\delta^{13}C$ in ‰ is not a conserved quantity. In fact, expressing CO_2 in terms of atmospheric response functions is also not perfect, because the response functions depend weakly on the level of CO_2 in the atmosphere (Joos et al., 1996). This simple model will, however, be shown to be quite valuable. Figure 5.6b shows atmospheric pulse responses for $\delta^{13}C$ from the BDM corresponding to a pulse of 1 GtC of biotic and

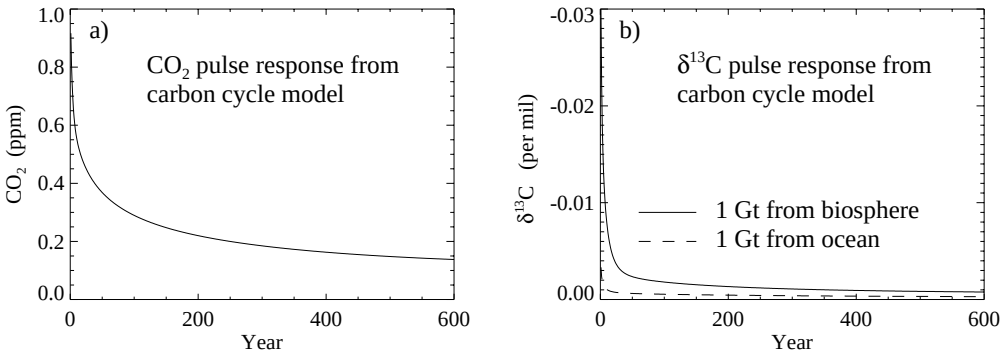

Figure 5.6: Pulse responses from the box diffusion model for a) CO_2 and b) $\delta^{13}C$. The response functions are calculated with the model parameters used in Section 4.4 by putting 1 GtC into the atmosphere.

oceanic CO_2. The response function for $\delta^{13}C$ due to CO_2 from the biosphere is

$$R_b(t) = -0.00072 - 0.03938\left[0.7575e^{-t/2.236} + 0.2153e^{-t/22.18} + 0.0272e^{-t/5681}\right] \quad (5.46)$$

and from the ocean

$$R_o(t) = -0.00028 - 0.00352\left[0.7341e^{-t/2.236} + 0.1854e^{-t/22.18} + 0.0805e^{-t/5681}\right] \quad (5.47)$$

The two $\delta^{13}C$ response functions have the same set of 'lifetimes', but different coefficients, so that $\delta^{13}C$ from either the biosphere or the ocean can be added to the same 'pools', in different proportions depending on its origin. The decay is much faster for $\delta^{13}C$ than for CO_2, as has been discussed in Section 2.5. The aim of using $\delta^{13}C$ as well as CO_2 is to partition uptake into oceanic and biotic components.

The equations for this model will be described with 2 state variables each for CO_2 and $\delta^{13}C$, although the calculations will have 4. There is one state variable for the net biospheric flux, and one for the net oceanic flux. The state is defined as

$$\mathbf{x} = \begin{bmatrix} C_1 \\ C_2 \\ \delta_1 \\ \delta_2 \\ \text{ocn} \\ \text{bio} \end{bmatrix} \quad (5.48)$$

The evolution matrix is

$$\Phi = \begin{bmatrix} e^{-\delta t/\tau_1} & 0 & 0 & 0 & \delta t\, a_1 e^{-\delta t/2\tau_1} & \delta t\, a_1 e^{-\delta t/2\tau_1} \\ 0 & e^{-\delta t/\tau_2} & 0 & 0 & \delta t\, a_2 e^{-\delta t/2\tau_2} & \delta t\, a_2 e^{-\delta t/2\tau_2} \\ 0 & 0 & e^{-\delta t/\tau_3} & 0 & \delta t\, b_1 e^{-\delta t/2\tau_3} & \delta t\, c_1 e^{-\delta t/2\tau_3} \\ 0 & 0 & 0 & e^{-\delta t/\tau_4} & \delta t\, b_2 e^{-\delta t/2\tau_4} & \delta t\, c_2 e^{-\delta t/2\tau_4} \\ 0 & 0 & 0 & 0 & 1 & 0 \\ 0 & 0 & 0 & 0 & 0 & 1 \end{bmatrix} \tag{5.49}$$

where τ_1 and τ_2 are the CO_2 'lifetimes', τ_3 and τ_4 are the $\delta^{13}C$ 'lifetimes', and the a_i, b_i and c_i are the coefficients for CO_2, biospheric $\delta^{13}C$ and oceanic $\delta^{13}C$, respectively. (For example, $b_1 = -0.03938 \times 0.7575$.)

Deterministic forcing, $\mathbf{u}$, has one component, corresponding to the fossil fuel source. This gives

$$\mathbf{u} = [\text{foss}] \tag{5.50}$$

and

$$\mathbf{G} = \begin{bmatrix} \delta t\, a_1 e^{-\delta t/2\tau_1} \\ \delta t\, a_2 e^{-\delta t/2\tau_2} \\ \delta t\, d_1 e^{-\delta t/2\tau_3} \\ \delta t\, d_2 e^{-\delta t/2\tau_4} \\ 0 \\ 0 \end{bmatrix} \tag{5.51}$$

where the d_i are the $\delta^{13}C$ response function coefficients for a pulse of fossil fuel CO_2. The source due to land-use change could also have been included as a component of the deterministic forcing.

The projection matrix for CO_2 and $\delta^{13}C$ observations is

$$\mathbf{H} = \begin{bmatrix} 1 & 1 & 0 & 0 & 0 & 0 \\ 0 & 0 & 1 & 1 & 0 & 0 \end{bmatrix} \tag{5.52}$$

Part of the ocean uptake of CO_2 and $\delta^{13}C$ is modelled by the response functions, so the source state variables give the remaining net ocean and biospheric fluxes required to match CO_2 and $\delta^{13}C$.

5.6.2 Q based on firn smoothing

The values of the stochastic forcing covariance (**Q**) for this calculation can be chosen based on a firn model calculation to quantify the CO_2 variations that survive smoothing due to the firn diffusion and trapping. A CO_2 record with typical annual variations was created using annual mean CO_2 concentrations from Mauna Loa between 1959 and 1995 (Keeling and Whorf, 1998). This 37 years of data, with the mean trend taken out, was added to the long term CO_2 increase from Law Dome between 1900 and 1995, with the Mauna Loa record repeated until the 95 years were covered (solid line in Figure 5.7a). The firn model was run for DE08 with this CO_2 record, giving the dashed line in Figure 5.7a. The year-to-year changes in concentration (in ppm) for the original and firn-modelled records are shown in Figure 5.7b. The year-to-year concentration changes at Mauna Loa are assumed to be of similar magnitude to the annual variations in global CO_2. The calculation was also run for the Mauna Loa variability without the Law Dome record (Figure 5.7c and 5.7d) to separate this from the variation due to the long term change. The year-to-year variations in the firn-smoothed concentrations are, as expected, much smaller than the variations in the original record. The maximum change in the firn-smoothed record is about 0.45 ppm over 10 years (around 1960 in Figure 5.7d). With 1 GtC = 0.47 ppm, this implies $q_{\rm src} = 0.45/0.47/\sqrt{10} = 0.3$ GtC yr^{-1} in a random walk model. Other parts of the record give values for $q_{\rm src}$ up to about this value. Based on this, a value of $\mathbf{Q} = 0.1$ (GtC yr^{-1})^2, corresponding to $q_{\rm src} = \sqrt{0.1} = 0.316$ GtC yr^{-1}, seems reasonable. This quantifies the variation that remains in the CO_2 record after smoothing due to the firn processes.

A similar calculation for δ^{13}C also supports the use of 0.1 (GtC yr^{-1})^2 for the biospheric flux. A consistent CO_2 and δ^{13}C record was created by running the annual CO_2 deviations shown by the solid line in Figure 5.7d (converted to GtC) as the land-use change flux (i.e. to/from the long-lived biospheric box) in a forward calculation of the BDM. The fossil fuel source was also used. The calculated CO_2 and δ^{13}C were then run in the firn model. The solid line in Figure 5.7e shows the δ^{13}C input to the firn model, and the short-dashed line shows the output δ^{13}C calculated with the ^{12}C diffusion coefficient, D_{12}, used for both the ^{13}C and ^{12}C tracers (OUTPUT1). This shows the smoothing without the effect of the different diffusion rates of ^{12}C and ^{13}C. δ^{13}C was also calculated with D_{13} used for

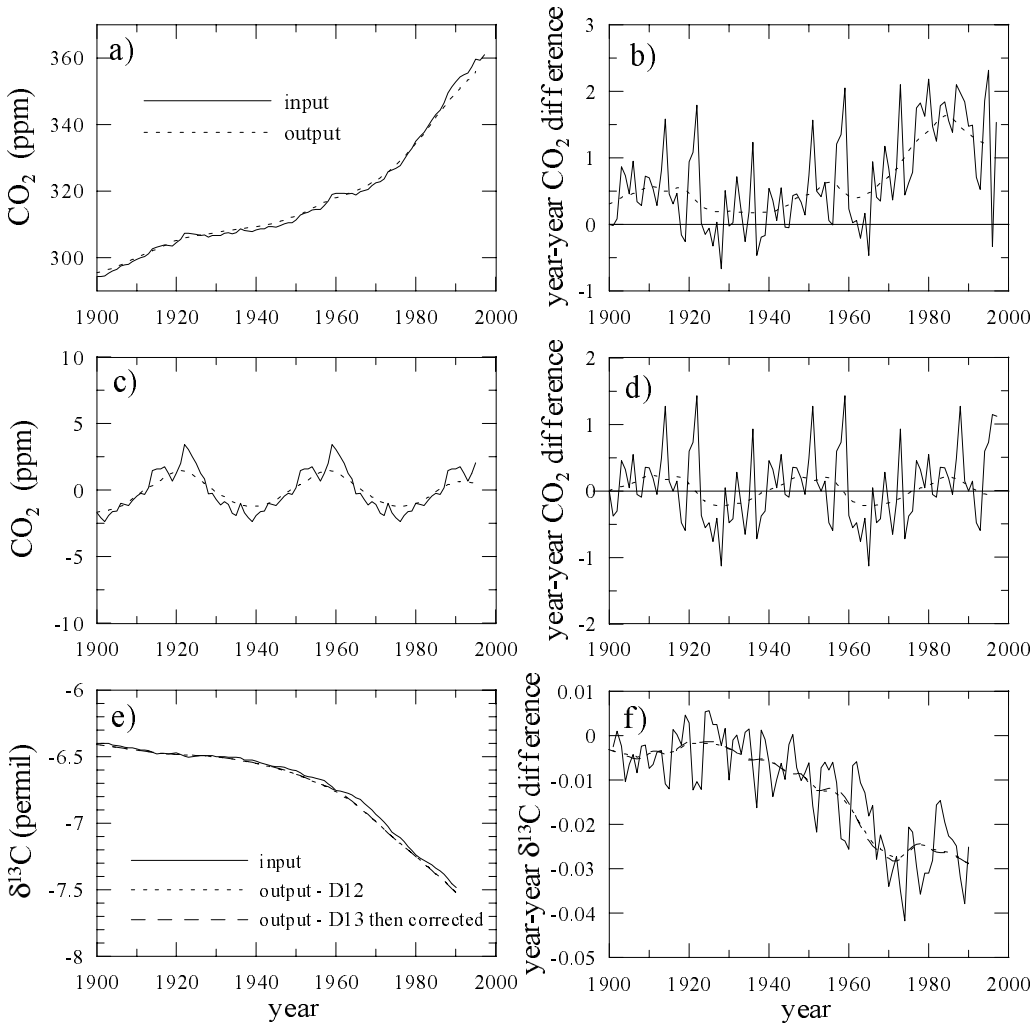

Figure 5.7: a) CO_2 record created by adding deviations of annual mean CO_2 concentrations from a linear increase at Mauna Loa to the Law Dome ice core record (solid line). The dashed line shows this record as it would be trapped in ice, determined with a firn model calculation for DE08. b) Year-to-year differences in CO_2 concentration (in ppm) for the 2 curves shown in a). c) Same as in a), but with just the Mauna Loa deviations from linear (i.e. without the Law Dome record). d) Year-to-year differences for curves in c). e) $\delta^{13}C$ atmospheric and firn-smoothed records. f) Year-to-year $\delta^{13}C$ differences. Dashed lines in e) and f) show the firn model output calculated when the solid line is used as input.

the ^{13}C tracer (OUTPUT2), and then corrected for diffusion with a diffusion correction calculated with OUTPUT2 and firn-smoothed CO_2 used in the firn model. The corrected record is shown by the long-dashed line in Figure 5.7e. (The difference between OUTPUT1 and the corrected OUTPUT2 occurs because the diffusion correction was calculated with smoothed CO_2 instead of the 'real' atmospheric CO_2 history. This is how the correction

is applied in reality (see Section 3.7.2) and the difference it makes is quite small.) The year-to-year differences for the 3 δ^{13}C curves are shown in Figure 5.7f. The maximum changes in the firn-smoothed records are about 0.004 ‰ yr^{-1} over 6 years or 0.017 ‰ yr^{-1} over 15 years. With 1 GtC = 0.47 ppm and assuming 1 ppm = 0.05 ‰ for biospheric exchange (see Section 2.5), the annual changes required in a random walk model would be $0.004/0.05/0.47/\sqrt{6} = 0.0695 = \sqrt{0.005}$ GtC yr^{-1} for the change over 6 years and $0.017/0.05/0.47/\sqrt{15} = 0.187 = \sqrt{0.035}$ GtC yr^{-1} for the change over 15 years. Based on these calculations, $q_{\mathrm{src}} = \sqrt{0.1}$ GtC yr^{-1} ($\mathbf{Q} = 0.1$ (GtC yr^{-1})^2) will be used for both the oceanic and biospheric source components in the Kalman filter. Of course the rate of change of CO_2 and δ^{13}C in the firn-smoothed record depends very much on the input record, but the intention with these calculations was to use inputs that reflect real atmospheric variations.

5.6.3 Results

Figure 5.8 shows the Kalman filter results for this model configuration (with the 4-term response functions). The net ocean flux is the sum of the oceanic flux state variable and the uptake given by the response functions. The biospheric flux is the total net flux between the atmosphere and the biosphere (i.e. including land-use change, fertilisation, variations due to climate and anything else). The Kalman filter result can be tested relative to the BDM which was used to generate the pulse response functions by running the deduced sources in the BDM. This tests how well the pulse response functions represent the carbon cycle, and is particularly important for δ^{13}C. Comparison of the CO_2 and δ^{13}C from the BDM and the Kalman filter output is shown in Figure 5.9. Over the industrial period there is a gradual divergence of the Kalman filter output from the BDM output, ending up with a difference of 1.3 ppm and 0.03 ‰ by 1990 (each around 2% of the total anthropogenic change). This will cause small errors in the partitioning of uptake over long time scales with the Kalman filter. On shorter time scales (e.g. multi-decadal) the Kalman filter model captures the variability almost exactly as in the BDM. This is very encouraging, and perhaps even a bit surprising for δ^{13}C.

The innovations and χ^2 for $\mathbf{Q} = 0.1$ (GtC yr^{-1})^2 are shown in Figure 5.10. Figures 5.10a and 5.10b show the innovations for CO_2 and δ^{13}C, with the dashed lines indicating the data uncertainties given by Etheridge et al. (1996) and Francey et al. (1999a). The solid

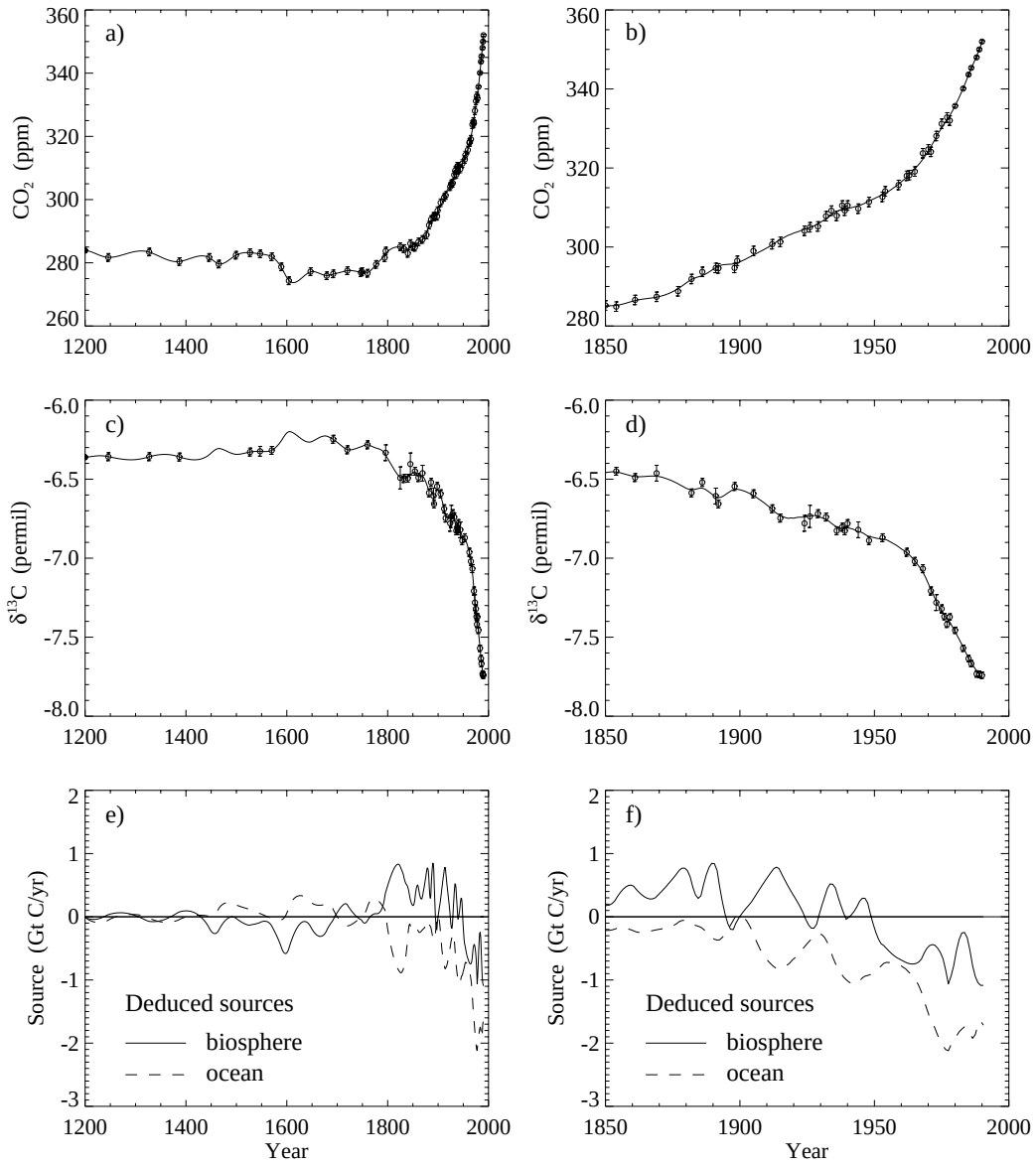

Figure 5.8: CO_2 concentration, $\delta^{13}C$ and deduced sources from the Kalman filter run with atmospheric pulse response functions. The uncertainties used were those given by Etheridge et al. (1996) for CO_2 and by Francey et al. (1999a) for $\delta^{13}C$. The ice core data were averaged where there were multiple concentrations in one year.

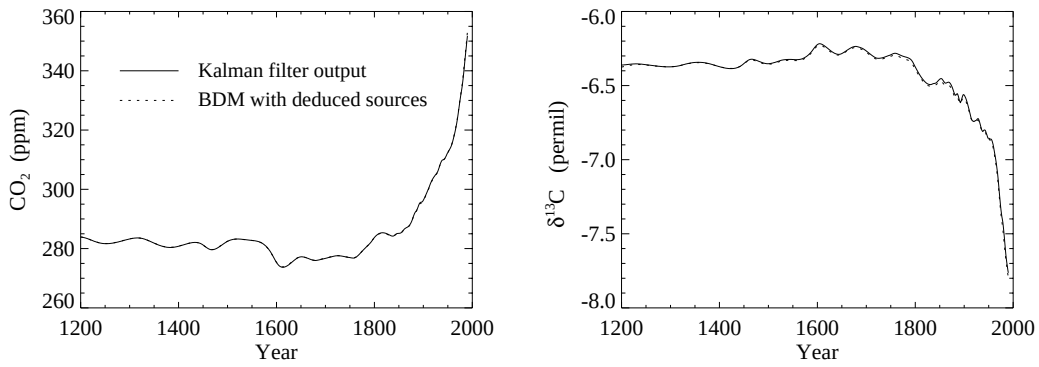

Figure 5.9: Comparison of the Kalman filter output (solid line) and the BDM run with the sources deduced by the Kalman filter (dashed line). The Kalman filter calculation used the atmospheric pulse response functions.

lines show the average innovations over the pre-industrial and industrial periods. In the industrial period, the CO_2 innovations are generally around or less than the magnitude of the CO_2 data uncertainties, while the $\delta^{13}C$ innovations are often greater than the $\delta^{13}C$ uncertainties. χ^2 is plotted for both CO_2 and $\delta^{13}C$ together (5.10c) and separately (5.10d and 5.10e). (The χ^2 for CO_2 and $\delta^{13}C$ together, shown in Figure 5.10c, was calculated as described in equation (5.42) then normalised by the number of degrees of freedom, which is the number of data items at that timestep, i.e. 2 when there is both CO_2 and $\delta^{13}C$ data and 1 when there is just CO_2 or $\delta^{13}C$.) In the pre-industrial period, χ^2 in each case is very close to zero. This is similar to the methane calculation, and occurs because the state covariance increases in the long data gaps. In the industrial period, the mean χ^2 for CO_2 is 0.45 and for $\delta^{13}C$ is 0.71. $\mathbf{Q}$ was chosen based on the firn model calculations and $\mathbf{R}$ used the published measurement uncertainties. Further tuning of these inputs using χ^2 will be described in Section 5.7.

5.6.4 Source uncertainties

An important feature of the Kalman filter calculation is that it estimates source uncertainties. The double deconvolution has two deduced source components, i.e. net fluxes with both the ocean and biosphere. As quite different processes control each of these fluxes, they may have different levels of variability as a function of frequency, for example the biospheric flux may be more variable than the oceanic flux on the interannual time scale

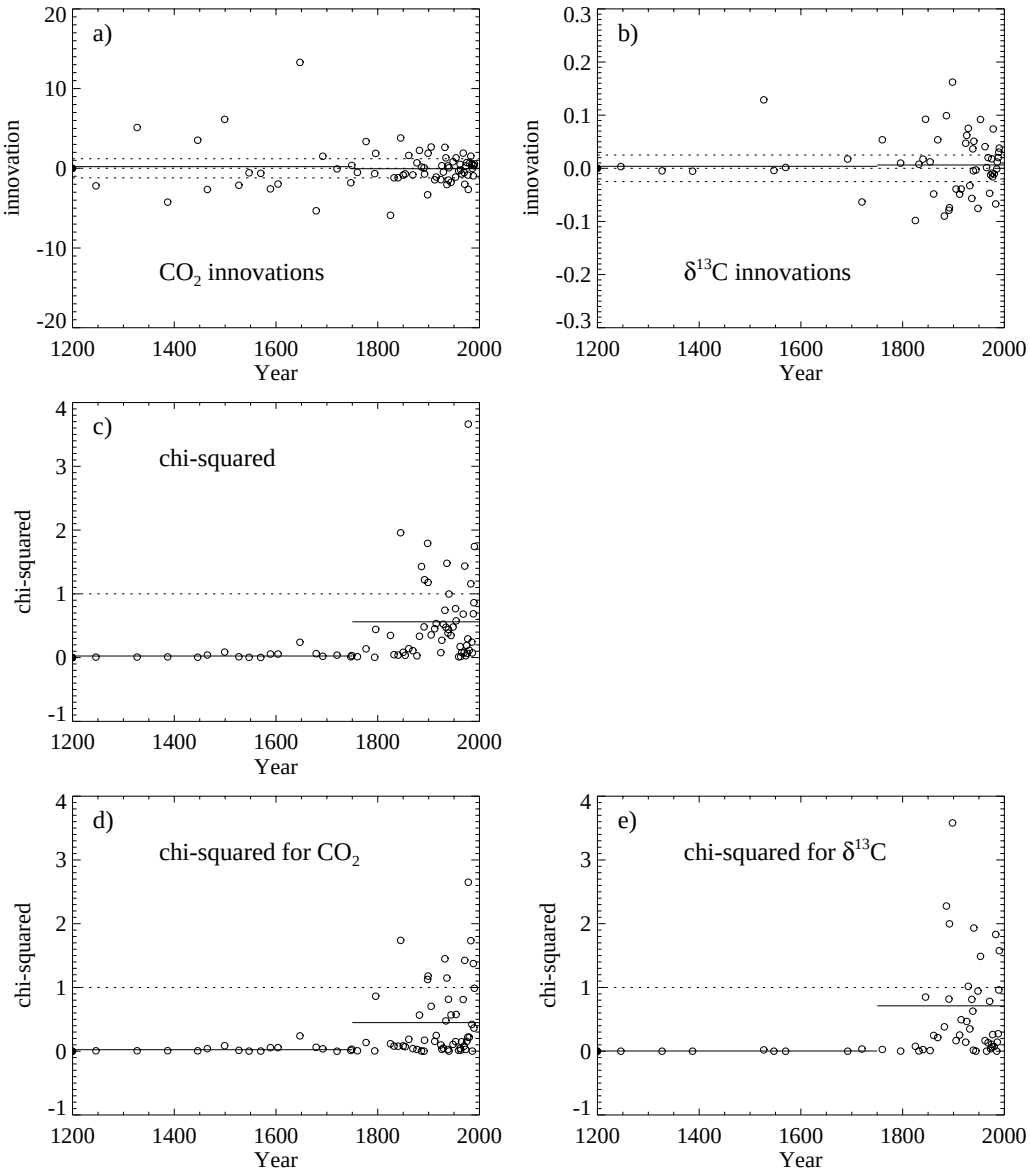

Figure 5.10: Innovations and χ^2 for CO_2 and $\delta^{13}C$ double deconvolution with atmospheric pulse response functions. **Q** is 0.1 for both net fluxes. a) Innovations for CO_2, b) innovations for $\delta^{13}C$, c) χ^2 for both CO_2 and $\delta^{13}C$, d) χ^2 for CO_2 and e) χ^2 for $\delta^{13}C$.

(see Section 4.4.3). In addition, even if the level of variability is similar, with the information contained in the CO_2 and $\delta^{13}C$ ice core records it may be possible to reconstruct the variation in one source better than in the other. This is, in fact, fairly likely to be the case, for the following reason. Broadly speaking, changes in CO_2 give the total net flux (ocean + biosphere) while $\delta^{13}C$ gives the biospheric flux. As $\delta^{13}C$ responds more to short term changes (e.g. decadal) than CO_2 (see Section 4.3.3), it may be that decadal variations in the biospheric flux are better reconstructed than the total flux or the oceanic flux. On longer time scales (centuries) the situation is probably the opposite with the total flux known better than the partition because CO_2 is better than $\delta^{13}C$ at reflecting long term changes (the pulse response functions in Figure 5.6 help illustrate that $\delta^{13}C$ responds to short time scales, and CO_2 more to long time scales). As for methane, the uncertainties for long term averages will be different from the uncertainties on short term variations, but in this case there may also be differences between uncertainties in the oceanic and biospheric components over the different time scales.

The square root of the calculated error variances of the state variables are shown in Figure 5.11, both over the full time range (left) and after 1850 (right). These standard deviations give the uncertainties on the state variables, so their evolution through the calculation tells us how well we know the calculated sources (and CO_2 and $\delta^{13}C$) at different times. As usual, uncertainties are generally lower near data points and higher between them. The uncertainty of the total flux (ocean + biosphere) is also calculated, and may be greater than or less than the ocean and biospheric fluxes individually, depending on whether the error correlation between ocean and biospheric fluxes is positive or negative (as indicated by the off-diagonal elements of the covariance matrix). The plot of flux uncertainties from 1850 onwards (Figure 5.11f) shows that (after 1850) the biospheric flux is known better than the oceanic flux or total flux. The oceanic flux uncertainty is smoother than the biospheric flux uncertainty, which is low very close to a $\delta^{13}C$ measurement, but increases rapidly between measurements. This reflects how, for the given $\mathbf{Q}$ and $\mathbf{R}$, $\delta^{13}C$ constrains the partition better than CO_2 constrains the total source at a data point, but due to the rapid decay of the $\delta^{13}C$ pulse, the $\delta^{13}C$ information doesn't extend very far in time. Similarly, the $\delta^{13}C$ uncertainty after 1850 (Figure 5.10d) appears more 'peaky' than the CO_2 uncertainty (Figure 5.10b). This is not due simply to differences in data density,

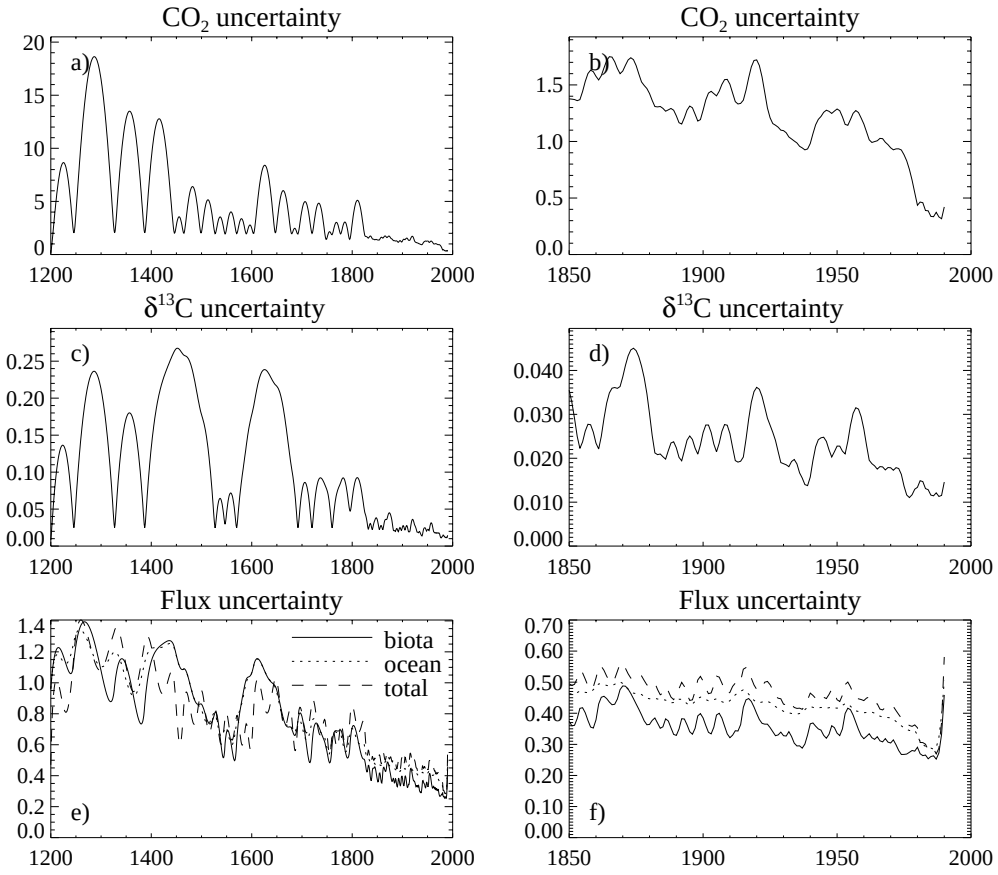

Figure 5.11: Calculated uncertainties for CO_2, $\delta^{13}C$ and the net fluxes from the Kalman filter double deconvolution with atmospheric pulse response functions.

as it is still seen in a calculation where both CO_2 and $\delta^{13}C$ have the same data density. The $\delta^{13}C$ record has two long gaps of more than 100 years where there are CO_2 measurements but no $\delta^{13}C$ (1388–1526 and 1571–1691). The plot of flux uncertainties (Figure 5.11e) shows that the total flux is known better than either the biospheric or oceanic flux in these long $\delta^{13}C$ data gaps. On the century time scale, $\delta^{13}C$ is not as useful at partitioning as CO_2 is at determining the total flux away from measurements. These characteristics of the error variances are as expected, and quantify the utility of CO_2 and $\delta^{13}C$ data in the calculation. The ability to perform this kind of analysis on the uncertainties is one of the important advantages of the Kalman filter deconvolution over the traditional mass balance deconvolution.

The flux uncertainties for the last year of the calculation are significantly higher than in the few years prior to the last year. This can be explained by considering what infor-

mation constrains the source estimates. Because the source is not 'observed', it must be estimated from changes in the concentrations that *are* observed. The source in year j is best determined by comparing concentrations in years $j+1$ and j. In this calculation, however, the source in the last year, $j = N$, is not able to use the concentration from the year $N+1$. In fact, in the whole forward pass of the Kalman filter, the source at each timestep is estimated without the most important piece of information – the concentration at the next timestep. Use of the Kalman smoother solves this problem, but not for the source at the last timestep, hence the large uncertainty. The source uncertainty at the final point (and for the whole forward pass) is determined by $\mathbf{Q}$. Without concentration data at time $j+1$, the best estimate of the source at time j will be by evolution of the source from the previous time, and this adds $\mathbf{Q}$ to the source variance. In Rayner et al. (2000, Section 4.3.1.1), we described a Kalman filter exercise with annual methyl chloroform data and a random walk evolution for the source. In this example, even with essentially perfectly known data (very small values in $\mathbf{R}$) the uncertainty on the source estimates from the forward pass are always greater than $\mathbf{Q}$. This illustrates the importance of the Kalman smoother for applications that estimate sources from concentrations.

The errors on the individual ice core measurements were given by Etheridge et al. (1996) as 1.2 ppm for CO_2 and by Francey et al. (1999a) as 0.025 ‰ for most of the $\delta^{13}C$, with slightly higher values for the remaining points (see Section 3.7.2). The calculations already described have used these values, and 0.3 ppm for CO_2 and 0.02 ‰ for $\delta^{13}C$ after 1980. The behaviour of the state variable uncertainties for different values of the data uncertainties will be explored in the next section. Estimates of the deduced sources are shown with uncertainties in Figure 5.12. Discussion of the sources and their uncertainties will also be given in the next section, along with the effect of the different values of $\mathbf{Q}$.

The main limitation of this model is the incorrect partitioning of uptake of anthropogenic CO_2 on the century time scale due to neglected nonlinearities. On time scales up to about a century the behaviour of the model is (perhaps surprisingly) remarkably good. Particular advantages of the model are that the equations are linear, and because the model is relatively simple, the results are easy to understand. Since the partitioning of uptake on the long time scale is important, a more complete approach will be developed in the next section.

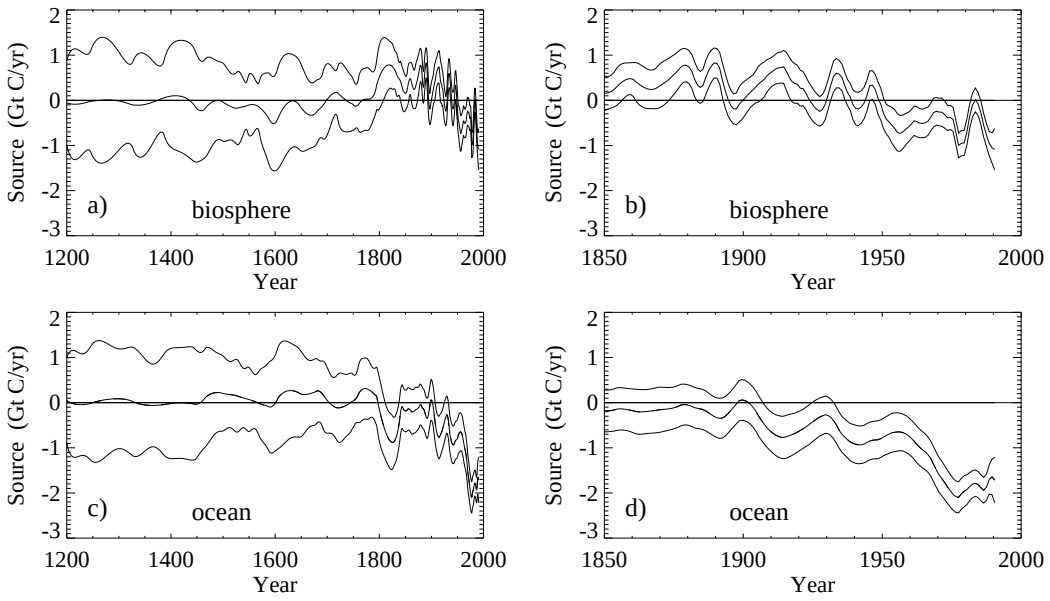

Figure 5.12: Deduced sources with uncertainties from the Kalman filter run with atmospheric pulse response functions and $\mathbf{Q} = 0.1$ (GtC yr^{-1})^2, shown over the full time range as well as just after 1850.

5.7 CO_2 and δ^{13}C: mixed layer pulse response functions

5.7.1 Model formulation

In this section, the double deconvolution calculations described in the previous section are repeated with a better model of the carbon cycle. There are two main problems with the model described in the previous section. Firstly, the atmospheric pulse response functions change as CO_2 increases in the atmosphere due to the nonlinearity of carbon chemistry when CO_2 exchanges between the atmosphere and the surface of the ocean. This will be addressed by using mixed layer pulse response functions (Joos et al., 1996) instead of atmospheric pulse functions, and modelling the exchange between the atmosphere and mixed layer explicitly. Joos et al. (1996) gives equations for the decay of a pulse of tracer in the mixed layer as it mixes into the deep ocean, calculated using a number of ocean models ranging from a box diffusion model to a 3-d ocean model. These equations can also apply for the isotopes of carbon, provided the isotopes are expressed in terms of conserved quantities. The other problem with the previous method is that δ^{13}C is modelled in permil,

which is not a conserved quantity. Instead, δ^{13}C will be modelled as an isotopic anomaly,

$$\mathrm{X} = \mathrm{C} \times \delta^{13}\mathrm{C} \tag{5.53}$$

in units of GtC ‰. This isotopic anomaly is a conserved quantity (Tans, 1980), and is approximately ^{13}C concentration. The equations for the evolution of the state are based on the CO_2 and $^{13}CO_2$ budget equations developed by Tans et al. (1993) and described in Section 2.5.

As in the deterministic form of the double deconvolution, ^{13}C is modelled in the biosphere and mixed layer only to provide estimates of the isotopic disequilibrium fluxes needed for the ^{13}C budget. The mixed layer response functions from Joos et al. (1996) are given as sums of exponentials, so are easily used in the autoregressive format described in the previous section, but now with 'pools' of CO_2 and the anomaly, X, in the mixed layer. The biosphere will be modelled essentially as it is in the BDM, with 2 boxes having the same sizes and gross fluxes as those used in Chapter 4. The size of the biospheric boxes (i.e. the amount of carbon) is kept constant in this calculation, in contrast to the BDM calculations where net fluxes of carbon alter the box sizes. This makes a very small difference to the calculated isofluxes (less than 1.5 GtC ‰ y^{-1} in 1990, compared to an overall change of about 90 GtC ‰ y^{-1}) but simplifies the equations considerably.

The state is defined as

$$x = \begin{bmatrix} \mathbf{Ca} \\ \mathbf{Xa} \\ \mathbf{Xb1} \\ \mathbf{Xb2} \\ \mathbf{Cs}_{1,n} \\ \mathbf{Xs}_{1,n} \\ \mathbf{Bi} \\ \mathbf{Oc} \end{bmatrix} \tag{5.54}$$

where **Ca** is the atmospheric CO_2 content in GtC, **Xa** is the isotopic anomaly in the atmosphere in GtC ‰, **Xb1** and **Xb2** are the isotopic anomalies in the short- and long-lived biospheric boxes in GtC ‰, and **Bi** and **Oc** are the net fluxes in GtC yr^{-1}. $\mathbf{Cs}_i$ and $\mathbf{Xs}_i$ are CO_2 and isotopic anomaly components in the mixed layer (in GtC and GtC ‰,

respectively), and $\mathbf{Cs}_{1,n} = (\mathbf{Cs}_1, \mathbf{Cs}_2, ..., \mathbf{Cs}_n)$, $\mathbf{Xs}_{1,n} = (\mathbf{Xs}_1, \mathbf{Xs}_2, ..., \mathbf{Xs}_n)$ and n is the number of components (each corresponding to an exponential in the response function). Equations for the evolution of the state, with state variables shown in bold, are given in Table 5.1. A description of the constants in the equations, with units and values, is given in Table 5.2. Isotopic anomalies are all modelled relative to the pre-industrial atmospheric δ^{13}C level, δa_{init}. Isotopic ratios for the atmosphere, mixed layer and biospheric boxes relate to the state variables as follows:

$$\delta a = \frac{\mathbf{Xa}}{\mathbf{Ca} + \text{Ca}_{\text{init}}} + \delta a_{\text{init}} \tag{5.55a}$$

$$\delta s = \frac{\sum_k \mathbf{Xs_k}}{\sum_j \mathbf{Cs_j} + \text{Cs}_{\text{init}}} + \delta s_{\text{init}} \tag{5.55b}$$

$$\delta b_1 = \frac{\mathbf{Xb1} + \text{Xb1}_{\text{init}}}{\text{Cb1}} + \delta a_{\text{init}} + \varepsilon_{ab} \tag{5.55c}$$

$$\delta b_2 = \frac{\mathbf{Xb2} + \text{Xb2}_{\text{init}}}{\text{Cb2}} + \delta a_{\text{init}} \tag{5.55d}$$

The initial δ^{13}C in the mixed layer determined by the BDM to be in equilibrium with the atmospheric value of $\delta a_{\text{init}} = -6.3611$ ‰ is $\delta s_{\text{init}} = 2.459$ ‰. The difference $\delta a_{\text{init}} - \delta s_{\text{init}} = -8.82$ ‰ is close to, but not equal to, the difference between the fractionation factors, $\varepsilon_{oa} - \varepsilon_{ao} = -8.78$ ‰. The Tans et al. (1993) equations suggest that they should be equal, but these equations specifying the fractionation factors as additive are only an approximation. The equations in the BDM expressing the fractionations as multiplicative are more exact, therefore the BDM δs_{init} value will be used.

The system of equations in Table 5.1 is nonlinear in the state variables. This complicates the situation, and requires use of the Extended Kalman filter (described in Section 5.2.3). Fortunately, though, the equations are not very nonlinear, as variations in the linearised evolution matrix with time are small and predictable. The number of terms in the mixed layer response functions given by Joos et al. (1996) is 7 for the box diffusion model and 6 for the other models. (The equations for the response functions in Joos et al. are given over 2 time ranges, and the longer one is used in these calculations). Joos et al. gave the response functions with a large number of terms to ensure that they are accurate for future projections of CO_2, and can handle the substantial increases in CO_2 that are expected in the future. This application doesn't need as many terms as given, because calculations are only run up to present day CO_2 levels. The expressions given by Joos et al. can be rewritten as 5 term expressions. The advantage of this is to reduce the size of

$$
\begin{aligned}
\mathbf{Ca} &= \mathbf{Ca} + \mathbf{Bi} + \mathbf{Oc} + \text{fossil} \\
\mathbf{Xa} &= \mathbf{Xa} + \mathbf{Bi}\left(\frac{\mathbf{Xa}}{\mathbf{Ca} + \text{Ca}_{\text{init}}} + \varepsilon_{ab}\right) + \mathbf{Oc}\left(\frac{\mathbf{Xa}}{\mathbf{Ca} + \text{Ca}_{\text{init}}} + \varepsilon_{ao}\right) + \text{fossil} \times (\delta_{\text{ff}} - \delta a_{\text{init}}) \\
&\quad + \phi_{\text{B1}} \frac{\mathbf{Xb1} + \text{Xb1}_{\text{init}}}{\text{Cb1}} + \phi_{\text{B2}} \frac{\mathbf{Xb2} + \text{Xb2}_{\text{init}}}{\text{Cb2}} - \phi_{\text{BT}} \frac{\mathbf{Xa}}{\mathbf{Ca} + \text{Ca}_{\text{init}}} - \phi_{\text{BT}} \varepsilon_{ab} \\
&\quad + (\mathbf{Ca} + \text{Ca}_{\text{init}})\, k_g \left[\frac{\sum_k \mathbf{Xs_k}}{\sum_j \mathbf{Cs_j} + \text{Cs}_{\text{init}}} - (\varepsilon_{ao} - \varepsilon_{oa})\left(\frac{\sum_k \mathbf{Cs_k}}{\sum_j \mathbf{Cs_j} + \text{Cs}_{\text{init}}}\right) - \frac{\mathbf{Xa}}{\mathbf{Ca} + \text{Ca}_{\text{init}}}\right] \\
\mathbf{Xb1} &= \mathbf{Xb1} + \phi_{\text{BT}}\left[\frac{\mathbf{Xa}}{\mathbf{Ca} + \text{Ca}_{\text{init}}} + \varepsilon_{ab} - \frac{\mathbf{Xb1} + \text{Xb1}_{\text{init}}}{\text{Cb1}}\right] \\
\mathbf{Xb2} &= \mathbf{Xb2} + \phi_{\text{B2}}\left[\frac{\mathbf{Xb1} + \text{Xb1}_{\text{init}}}{\text{Cb1}} - \frac{\mathbf{Xb2} + \text{Xb2}_{\text{init}}}{\text{Cb2}}\right] \\
\mathbf{Cs_i} &= \mathbf{Cs_i} e^{-\frac{\Delta t}{\tau_i}} - \mathbf{Oc} \times a_i e^{-\frac{\Delta t}{2\tau_i}} \\
\mathbf{Xs_i} &= \mathbf{Xs_i} e^{-\frac{\Delta t}{\tau_i}} - \mathbf{Oc}\left(\frac{\mathbf{Xa}}{\mathbf{Ca} + \text{Ca}_{\text{init}}} + \varepsilon_{ao}\right) \times a_i e^{-\frac{\Delta t}{2\tau_i}} \\
&\quad - (\mathbf{Ca} + \text{Ca}_{\text{init}})\, k_g \left[\frac{\sum_k \mathbf{Xs_k}}{\sum_j \mathbf{Cs_j} + \text{Cs}_{\text{init}}} - (\varepsilon_{ao} - \varepsilon_{oa})\left(\frac{\sum_k \mathbf{Cs_k}}{\sum_j \mathbf{Cs_j} + \text{Cs}_{\text{init}}}\right) - \frac{\mathbf{Xa}}{\mathbf{Ca} + \text{Ca}_{\text{init}}}\right] \\
&\quad \times a_i e^{-\frac{\Delta t}{2\tau_i}} \\
\mathbf{Bi} &= \mathbf{Bi} \\
\mathbf{Oc} &= \mathbf{Oc}
\end{aligned}
$$

Table 5.1: Evolution equations for the double deconvolution with mixed layer response functions.

	value	units	description
Ca_{init}	283.9 × 2.1276	GtC	initial atmospheric CO_2 content
Xb1_{init}	-18 × 140	GtC ‰	initial anomaly in biospheric box 1
Xb2_{init}	-18 × 1400	GtC ‰	initial anomaly in biospheric box 2
Cs_{init}	679	GtC	initial mixed layer CO_2 content
Xs_{init}	8.82 × 679	GtC ‰	initial mixed layer anomaly
ϕ_{B1}	76.67	GtC yr^{-1}	gross flux from biosphere box 1 to atmosphere
ϕ_{B2}	23.33	GtC yr^{-1}	gross flux from biosphere box 2 to atmosphere
ϕ_{BT}	$\phi_{\text{B1}} + \phi_{\text{B2}}$	GtC yr^{-1}	gross flux from atmosphere to biosphere box 1
ε_{ao}	-2.05	‰	air-sea fractionation
ε_{oa}	-10.83	‰	sea-air fractionation
ε_{ab}	-18.0	‰	air-biosphere fractionation
τ_i	Joos et al.	yr	lifetimes from mixed layer response functions
a_i	Joos et al.	–	coefficients from m. l. response functions
k_g	Joos et al.	yr^{-1}	gas exchange coefficient
fossil	0.0 – 6.1	GtC yr^{-1}	timeseries of the source due to fossil fuel
δ_{ff}	24.1 – 28.2	‰	timeseries of fossil fuel δ^{13}C
δa_{init}	-6.3611	‰	initial atmospheric δ^{13}C

Table 5.2: Description and values of many of the constants in the equations in Table 5.1.

the covariance matrix, P, in the calculation, and the difference this makes to the results of the model is negligible. Even with the smaller number of terms this still gives 16 state variables. The backward pass of the 2-pass and RTS smoothers require the covariance matrix from the forward pass (a 16×16 matrix) to be inverted. The condition number of the covariance matrix from the forward pass is often larger than 10^{11}, indicating problems for calculating the inverse. This is mainly due to the size of the matrix, as there are now many state variables, but is worst at the end of a big gap in the observations, when the uncertainty on the state estimates (and therefore the elements in P) are greatest. The Bryson-Frazier smoother equations (Section 5.2.2), which don't involve inversion of the covariance matrix, are therefore required.

This application of the Kalman filter uses the δ^{13}C data (and their uncertainties) expressed as isotopic anomalies. The Kalman filter could also have been set up to include the δ^{13}C data in permil. As δ^{13}C in permil is a nonlinear function of the state variables C and X, the projection equation (equation (5.36)) would need to be linearised as described in Section 5.2.3. If there were any δ^{13}C data without corresponding CO_2 it would be necessary to formulate the model in this way. However, since the ice core record has CO_2 wherever δ^{13}C is measured, δ^{13}C data are used as anomalies.

In a small number of cases there are more than one CO_2 or δ^{13}C measurement for a single year. These measurements have been averaged and used in the Kalman filter with the original uncertainty. Instead of averaging, all of the measurements could have been included as data in the Kalman filter, by altering the projection matrix to allow more than one measurement of the concentration or δ^{13}C for a single time. This would improve the statistics, and also give a feel for how scattered measurements can be for a single year. However, since only a small number of times are involved (less than 16 %) this was not done. If data are averaged, the data uncertainty should be reduced compared with the original uncertainty (by dividing by the square root of the number of measurements averaged). The data uncertainties will be altered in Section 5.7.3 to explore different cases, and this would complicate the calculations so is not done.

The isotopic anomaly in the mixed layer is modelled in order to calculate the isoflux, and as part of that, carbon in the mixed layer (**Ca**) is calculated. In theory, an estimate of the air-sea exchange, F_{as}, could be calculated from the modelled air-sea partial pressure

difference as

$$F_{\rm as} = k_g \mathbf{Ca} - \frac{\xi k_g {\rm Ca}_{\rm init}}{{\rm Cs}_{\rm init}} \sum_k \mathbf{Cs_k} \tag{5.56}$$

(where ξ is the buffer factor and k_g the gas exchange coefficient) and the state variable, **Oc**, would be the additional ocean source required to match the ice core records. The calculation was initially formulated in this way, but then changed for the following reason, so that **Oc** is the total ocean flux. In the end we want to determine the total ocean flux, whether this is **Oc** on its own or $\mathbf{Oc} + F_{\rm as}$, however the two cases do differ. The ice core record is characterised by long gaps in the data. In these gaps the forward pass of the Kalman filter proceeds using the evolution equation. If $F_{\rm as}$ is not calculated, the total air-sea flux (**Oc**) does not change until a new data point is reached, often causing the amount of CO_2 in the atmosphere and mixed layer to diverge. If $F_{\rm as}$ is calculated, it can respond to changes in the atmospheric and mixed layer CO_2, but **Oc** still cannot. This results in $F_{\rm as}$ roughly mirroring **Oc** in the evolution step because **Ca** and $\sum_k \mathbf{Cs_k}$ depend on $F_{\rm as} + \mathbf{Oc}$, and $F_{\rm as}$ depends on **Ca** and $\sum_k \mathbf{Cs_k}$. This leads to a strong anticorrelation between **Oc** and $F_{\rm as}$ on the forward pass. The smoother probably doesn't see a problem with the anticorrelation on the backward pass, so doesn't change it much. Neither case is perfect, but the case without $F_{\rm as}$ is simpler to implement and understand and there appears to be no advantage in calculating $F_{\rm as}$. The mixed layer is modelled only for the isofluxes, which are not very sensitive to which case is used. The atmospheric pulse response function calculation of the previous section is more like the 'no $F_{\rm as}$' case, as the total ocean flux stays constant without new data.

The Kalman filter results can be checked relative to the model used to create the pulse response functions by using mixed layer pulse response functions from the BDM in the Kalman filter, then running the estimated sources in the BDM. This will check the whole system (including the mixed layer response functions). The Extended Kalman filter and the Bryson-Frazier smoother can be checked by running a forward calculation with the estimated sources and the mixed layer response functions. Both tests give excellent agreement, confirming that the Extended Kalman filter and the Bryson-Frazier smoother are behaving as required for this (weakly nonlinear) application.

5.7.2 Results

Figure 5.13 shows the double deconvolution results for the Kalman filter calculation using mixed layer response functions. The fluxes shown are **Oc** and **Bi**, which are the total fluxes between the atmosphere and the oceans and terrestrial biosphere (the response functions in this case model mixing from the mixed layer to the deep ocean). The case shown has $\mathbf{Q} = 0.1$ (GtC yr^{-1})^2, data uncertainties given by Etheridge et al. (1996) and Francey et al. (1999a) and the mixed layer response functions for the BDM described in Chapter 4. The results for the mixed layer response function (MLRF) double deconvolution look quite similar to the atmospheric response function (ARF) double deconvolution. They differ mainly on the long time scale because the response functions give different overall partitioning of CO_2 uptake. Both calculations have a rather unbelievable anticorrelated peak in the biospheric and oceanic fluxes just after 1800. This is around the beginning of the DE08 and DE08-2 records, and will be discussed in Chapter 6.

Figure 5.14a shows the time evolution of CO_2 in the atmosphere and mixed layer for the MLRF calculation. Recall that the difference between these quantities (i.e. ΔpCO_2) is *not* used to calculate air-sea exchange, and the difference will not necessarily be consistent with the deduced flux. (This is also the case in the mass balance double deconvolutions by Joos and Bruno (1998)). The ocean and biosphere are modelled only for the isofluxes, which are shown in Figure 5.14b. Sensitivity of the isofluxes to different ocean and biospheric models will be discussed in Chapter 6. Figure 5.14c shows the variation of $\delta^{13}C$ in the atmosphere and mixed layer.

In the forward pass of the Kalman filter, the CO_2 and $\delta^{13}C$ can wander off track in the long data gaps. As the model is slightly nonlinear, the evolution matrix depends on these values of CO_2 and $\delta^{13}C$. To avoid this introducing errors, the Kalman filter and smoother combination is run twice for each calculation, the first time linearising about the current trajectory and the second time linearising about the previous smoother solution. The difference this makes turns out to be very small.

The source uncertainties calculated by the Kalman filter are due to data error (**R**) and source evolution error (**Q**). Not included is the carbon-cycle-model error, i.e. how concentrations and sources are related, and how concentrations (and isotopes) evolve in time. The carbon cycle model is basically the same model that has been used in many

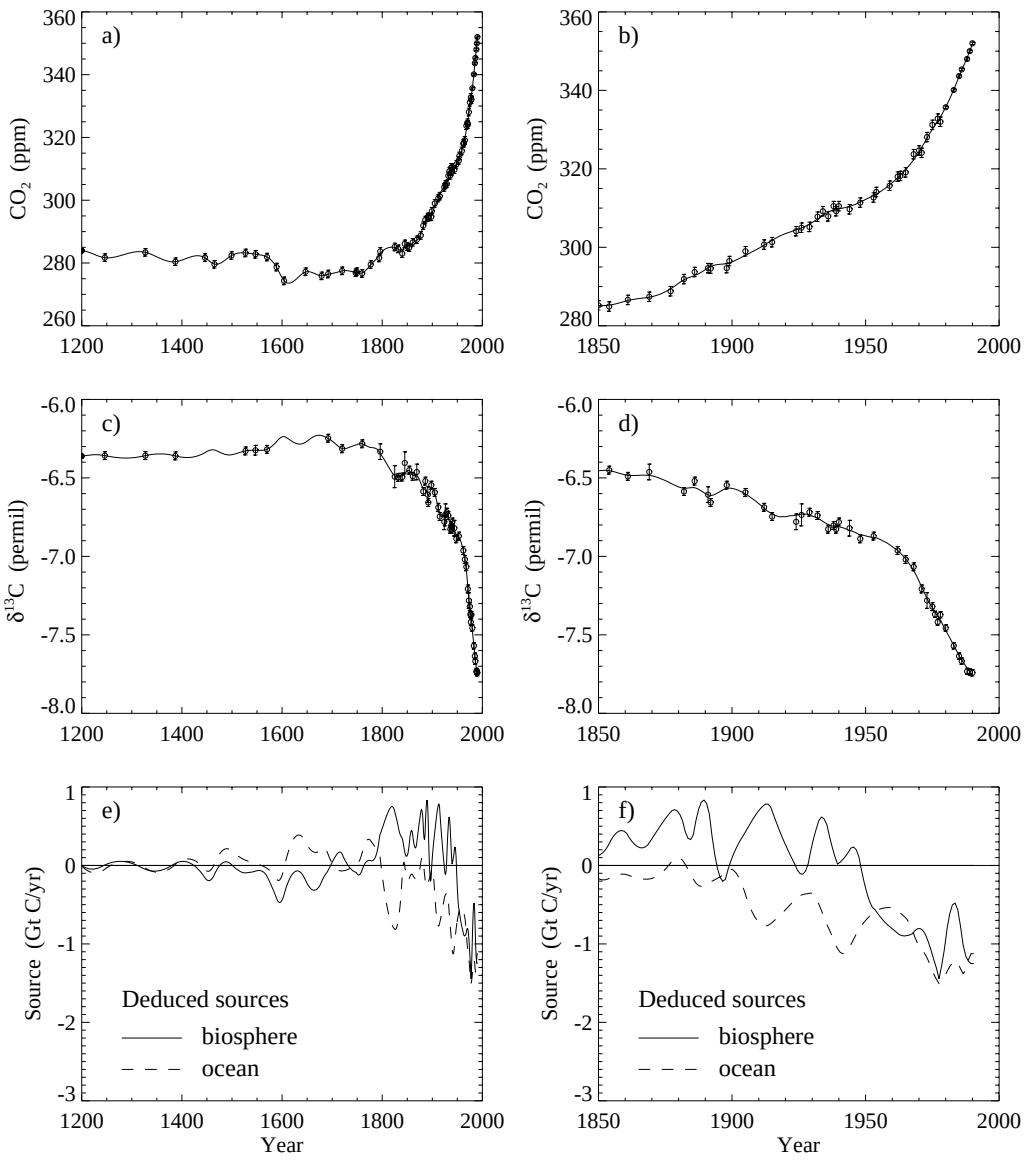

Figure 5.13: CO_2 concentration, $\delta^{13}C$ and deduced sources from the Kalman filter run with mixed layer pulse response functions. The data uncertainties used were those given by Etheridge et al. (1996) for CO_2 and by Francey et al. (1999a) for $\delta^{13}C$, and $\mathbf{Q} = 0.1$ $(\text{GtC yr}^{-1})^2$ for both source components.

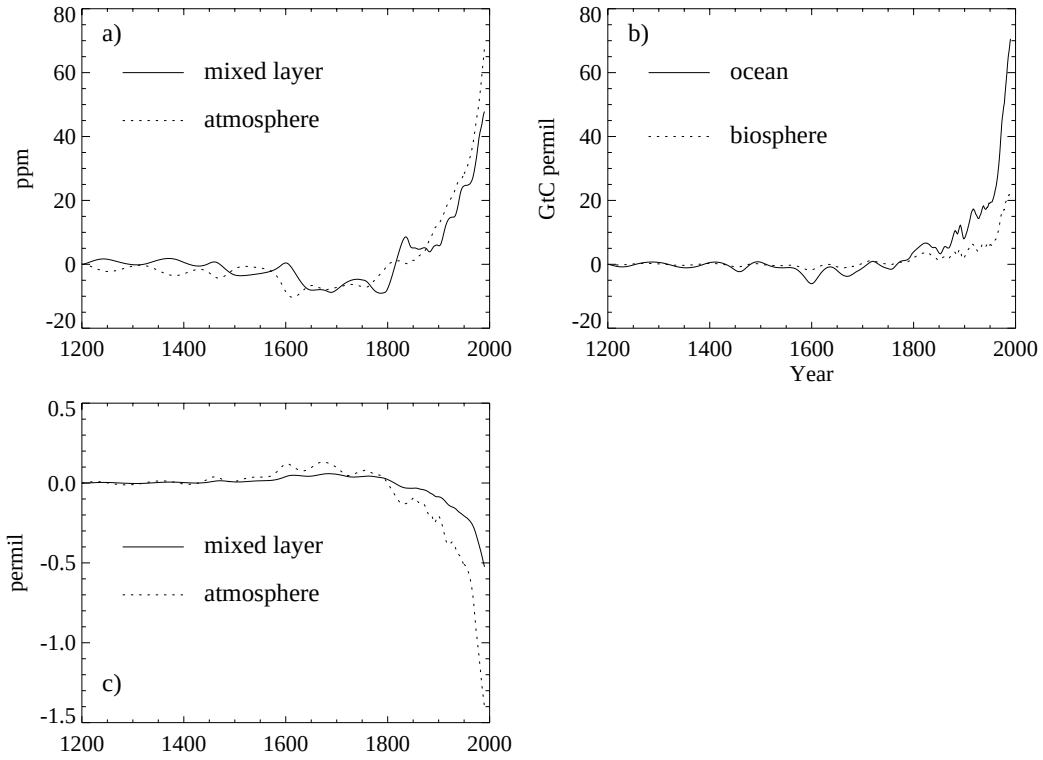

Figure 5.14: a) CO_2 in the atmosphere and pCO_2 in the mixed layer relative to initial levels from the standard MLRF double deconvolution calculation. b) Isotopic disequilibrium fluxes (isofluxes) from this calculation. c) $\delta^{13}C$ of the atmosphere and mixed layer in permil, plotted as a deviation from initial values.

deconvolution-type studies, and discussed in the previous chapter. The carbon-cycle-model errors are mainly relevant to the isofluxes (as they are the reason why the ocean and biospheric models are used), and these are discussed in other chapters. The source uncertainty due to systematic errors in the ice core data, e.g. the pre-industrial–modern difference, has not been included in the Kalman filter, but can be tested separately and is also discussed in other chapters. The part of the calculation that needs most validation is the statistics that go into the Kalman filter (i.e. $\mathbf{Q}$ and $\mathbf{R}$), and how these affect variability of CO_2, $\delta^{13}C$ and the fluxes. This can be dealt with to a fair degree by looking at the innovations and χ^2.

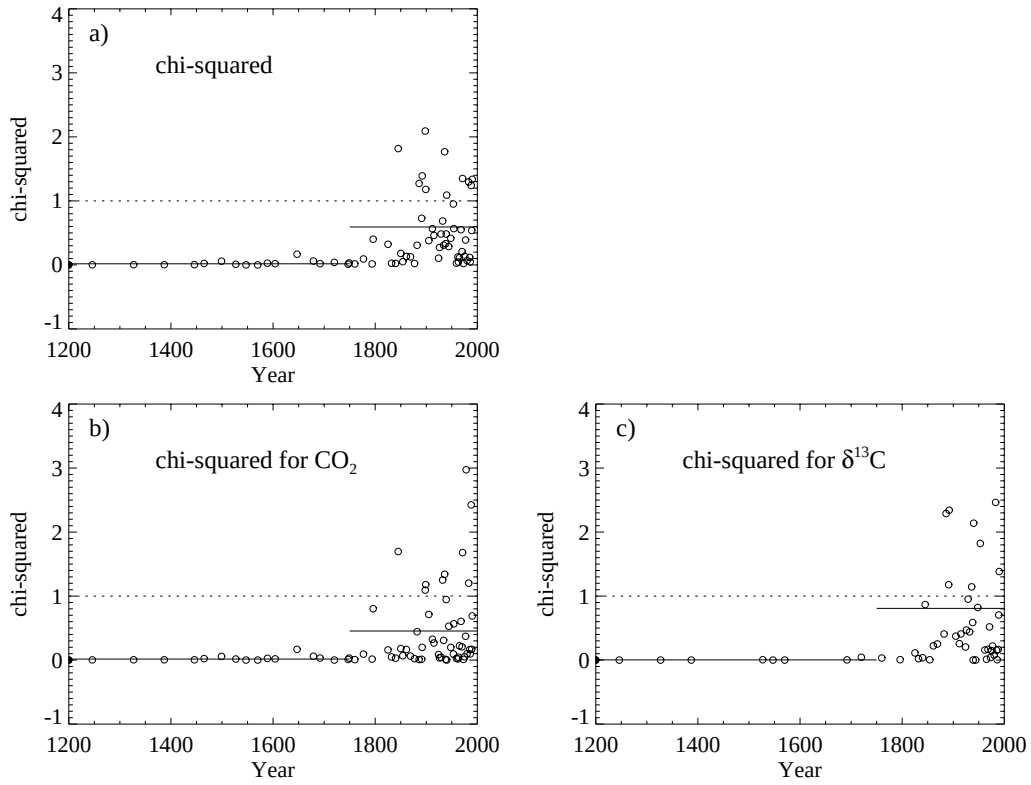

Figure 5.15: Chi-squared for CO_2 and the anomaly X from the double deconvolution with mixed layer pulse response functions.

5.7.3 Statistics

The statistics of the calculation over the industrial period will be examined in this section. Figure 5.15 shows chi-squared for the CO_2 and anomaly, X, both together and separately. The average of the χ^2 over the industrial period for CO_2 is 0.45 (the same as for the ARF calculation) and for X is 0.81. Another way to test the statistics of the calculation is to look at the distribution of the normalised residuals, i.e. the mismatch between the smoother solution and the data, normalised by the data uncertainty. Figure 5.16a and 5.16b show the distribution of normalised residuals for CO_2 and X, respectively, for data after 1800. The normalised residuals before 1800 are mostly very close to zero, and cause a large peak around zero if included in the distribution. The cumulative normalised residuals for CO_2 and X, along with the cumulative normal distribution (dashed line) are shown in Figure 5.16c and 5.16d.

Ideally, we want the mean χ^2 close to 1.0 and the normalised residuals to follow a

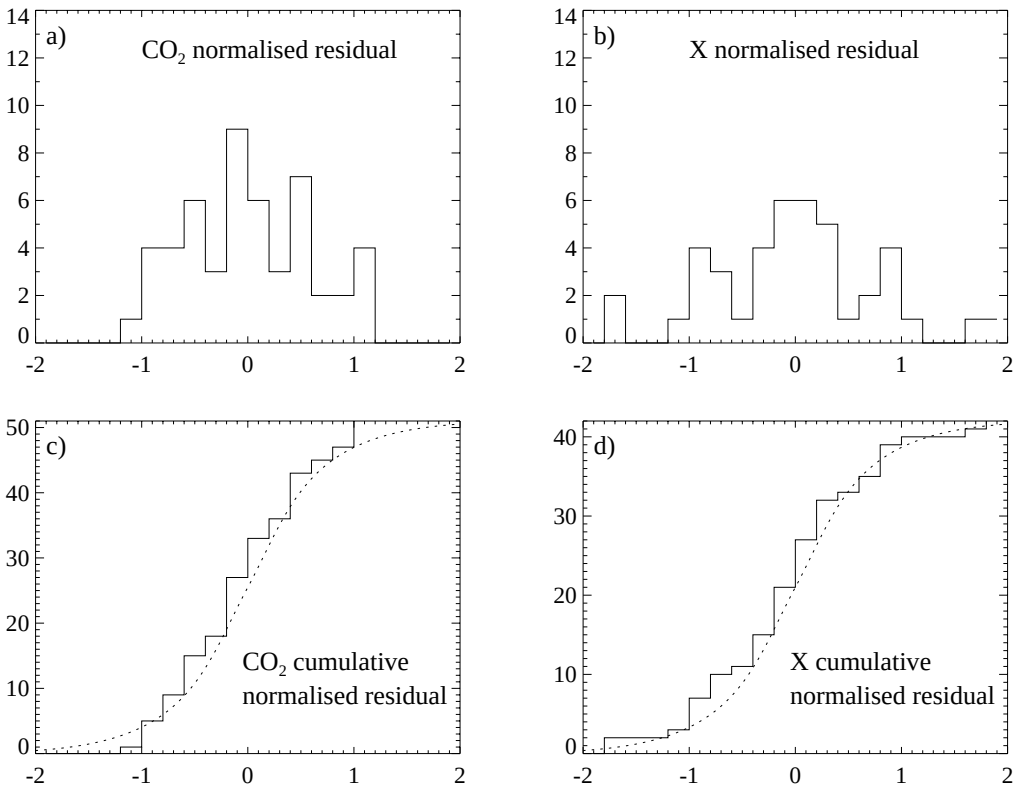

Figure 5.16: Distribution of normalised residuals for a) CO_2 and b) X. Cumulative normalised residuals for c) CO_2 and d) X. The dashed line shows the cumulative normal distribution.

Gaussian distribution for the Kalman filter to behave at its best. Due to the small number of data points, we can't expect the model to satisfy these constraints exactly. The normalised residuals for X are similar to the Gaussian distribution, but the residuals for CO_2 are all between -1.2 and 1.2, and therefore narrower. The mean χ^2 for CO_2 is also a fair way from 1.0. Based on these observations, and characteristics of the ice core measurements and their uncertainties, a case can be made for reducing the uncertainties on the CO_2 measurements. The CO_2 uncertainties of 1.2 ppm are quite conservative, and reflect the variation of CO_2 in multiple measurements sampled from one annual layer of ice (Etheridge et al., 1996). The uncertainty is much greater than the measurement precision for CO_2. The $\delta^{13}C$ uncertainties are closer to the measurement precision for $\delta^{13}C$. With the published uncertainties, the Kalman filter fits the decadal time scale features in $\delta^{13}C$ over the industrial period (Figure 5.13d) but not those in CO_2 (Figure 5.13b). The

CO_2 features are much smaller (relative to the industrial change) than the $\delta^{13}C$ features, which is expected to some extent. $\mathbf{Q}$ is large enough that the model can easily fit the CO_2 variations, but the data uncertainties are big enough that it doesn't need to. An important point is that features should be defined by more than one or two measurements for it to be desirable that the model fit them.

The Kalman filter run with the same $\delta^{13}C$ data uncertainties and $\mathbf{Q}$ as used previously, but with CO_2 uncertainties of 0.6 ppm (half of that given by Etheridge et al. (1996)) gives an average χ^2 over the industrial period of 1.03 for CO_2 and 0.83 for $\delta^{13}C$, with 0.99 for both together. The normalised residuals for CO_2 are also more widely spread than before, and closer to the Gaussian distribution. The CO_2, $\delta^{13}C$ and fluxes for these inputs are shown in Figure 5.17a, 5.17b and 5.17c. The model now tracks the CO_2 more closely. The fit to the $\delta^{13}C$ is similar to before. The main difference in the fluxes is that the variations in the ocean flux are now larger. This case will be treated as a standard case, known as DD1 and discussed in detail in the next chapter. It should be viewed as an example that pushes the ice core data to its limits. The data uncertainties suggest that the decadal features in the CO_2 and $\delta^{13}C$ records are real, and the model inverts them for the net fluxes. Further ice core measurements over this period are needed to confirm these features in both CO_2 and $\delta^{13}C$.

The more conservative approach of improving the model statistics by increasing the $\delta^{13}C$ uncertainties, rather than decreasing the CO_2 uncertainties, will also be investigated. The $\delta^{13}C$ uncertainties given by Francey et al. (1999a) may, in fact, have been too optimistic. If these $\delta^{13}C$ uncertainties are doubled (giving 0.05 ‰ for much of the data) and with $\mathbf{Q} = 0.1$, the model gives an average χ^2 of 0.42 for CO_2 and 0.29 for $\delta^{13}C$. The normalised residuals are generally between -1 and 1 for both CO_2 and $\delta^{13}C$, i.e. narrower than the Gaussian distribution. The CO_2, $\delta^{13}C$ and fluxes for this case are shown in Figure 5.17d, 5.17e and 5.17f. The χ^2 means are lower than we would like. Decreasing $\mathbf{Q}$ would increase the smoothing and have the effect of increasing the average χ^2 and widening the normalised residual distribution. However it was found that $\mathbf{Q}$ needs to be decreased to a very small value to give an average χ^2 near 1.0 for the larger data uncertainties. The small $\mathbf{Q}$ value required means that decadal features are not resolved and that the model essentially fits longer time scale variations. The $\mathbf{Q}$ of 0.1 is the magnitude

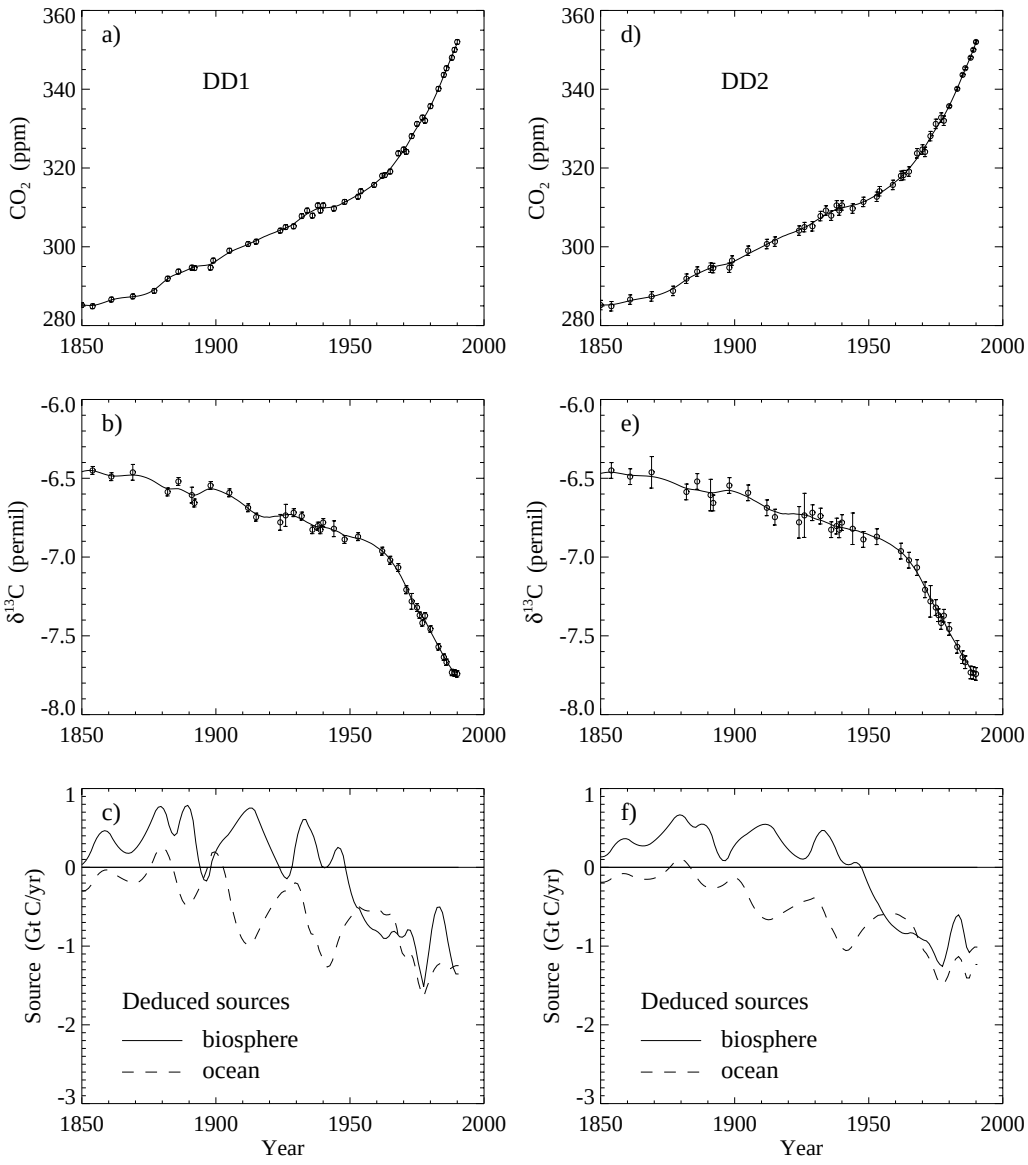

Figure 5.17: CO_2 concentration, $\delta^{13}C$ and deduced sources from the Kalman filter run with mixed layer pulse response functions. a), b) and c) are for DD1, the calculation with CO_2 data uncertainties of 0.6 ppm (half the published value from Etheridge et al. (1996)), and the $\delta^{13}C$ data uncertainties published by Francey et al. (1999a). d), e) and f) are for DD2, with the published CO_2 uncertainties and twice the Francey et al. (1999a) $\delta^{13}C$ uncertainties. Both calculations use $\mathbf{Q} = 0.1$ (GtC yr^{-1})^2 for both source components.

of the variations that survive firn smoothing, but the model suggests that with the larger, more conservative data uncertainties, they are not well resolved.

Even though the average values of χ^2 are not close to 1.0 for the calculation with larger data uncertainties and $\mathbf{Q} = 0.1$, the calculation is still acceptable. A large value of χ^2 is a sign of a more serious problem than a small χ^2. If χ^2 is greater than 1.0, the filter has a discrepancy between the uncertainty on the state and the uncertainty on a new measurement, believing that the state uncertainty is too small to accommodate the new measurement. If χ^2 is significantly less than 1.0, the state uncertainty is large enough to easily accommodate new measurements. The Jazwinski filter (Section 5.4) increases the state uncertainty if (effectively) χ^2 is greater than 1.0 but leaves it if χ^2 is less than 1.0. Whereas large χ^2 is a sign that the model is inconsistent, small χ^2 is a sign that it is perhaps too conservative, and that the data are not good enough (too sparse or too uncertain) to estimate the state as well as might otherwise be possible. The calculation with the published CO_2 uncertainties, doubled $\delta^{13}C$ uncertainties and $\mathbf{Q} = 0.1$ will be treated as a second standard case, referred to as DD2, and described in the next chapter.

The mean χ^2 is higher for CO_2 than for $\delta^{13}C$ in DD2. If the $\delta^{13}C$ uncertainties are increased by 50 % instead of doubled, then the average χ^2 is 0.43 and 0.45 for CO_2 and X, respectively. Such a calculation would have the advantage of similar average χ^2 for CO_2 and X, but differs less from DD1, so was not chosen as a standard calculation. The results are similar to DD2, but with larger amplitudes on the decadal variations.

The two cases, DD1 and DD2, are preferred to the case with the published uncertainties because they both have similar average χ^2 values and normalised residual distributions for CO_2 and $\delta^{13}C$, indicating that they draw information fairly equally from both types of measurement. An important justification for using different measurement uncertainties to those published is that the published CO_2 and $\delta^{13}C$ uncertainties were determined by different authors, and reflect different levels of confidence in the measurements. The temporal patterns of source variation in the two calculations are quite similar, it is mainly the magnitudes that vary. There is more suggestion of anticorrelation of the oceanic and biospheric fluxes in DD1.

If the uncertainties used in the DD1 calculation reflect the real uncertainties in the measurements, then this calculation is quite important. The average χ^2 is very close

to 1.0, and roughly the right proportion of normalised residuals are outside 1σ. Thus the innovations and normalised residuals are behaving exactly as we would like. This is consistent with there being variations in the CO_2 and $\delta^{13}C$ measurements that the firn model suggests should be seen in a firn-smoothed ice core record. If the uncertainties used in the DD1 calculation reflect the real uncertainties in the measurements, then the Kalman filter is behaving optimally. If the uncertainties used in DD1 are too optimistic for the present measurements, then this calculation shows what is possible (i.e. how precisely sources can be estimated) with those data uncertainties. In fact, even more than that, it shows what data uncertainties are required (with the given data density) for the double deconvolution to resolve features that the firn model believes may exist in the ice core record. The physics of the problem and the statistics of the Kalman filter are giving a consistent picture.

A third standard calculation, DD3, is designed to give century scale variations by using a small $\mathbf{Q}$. Figure 5.18 shows a calculation with published CO_2 uncertainties, doubled $\delta^{13}C$ uncertainties and $q_{\rm src} = \sqrt{0.001} = 0.032$ GtC yr^{-1}. The results of this calculation, as well as DD1 and DD2, will be described in the next chapter.

5.7.4 Source uncertainties

Flux uncertainties from the original MLRF calculation using the published data uncertainties and $\mathbf{Q} = 0.1$ (GtC yr^{-1})^2 are shown in Figures 5.19a and 5.19b. The flux uncertainties for the MLRF and ARF calculations are very similar, except for the biospheric flux uncertainty before about 1400. The MLRF calculation, which suggests that the biospheric flux is known better than the total flux for the given parameters, is probably more reliable than the ARF calculation because of the better treatment of $\delta^{13}C$ in the MLRF model. The biospheric flux uncertainty is still higher than the total flux uncertainty in the two long $\delta^{13}C$ data gaps mentioned in the previous section. Figures 5.19c and 5.19d show the flux variances for the DD1 calculation, and Figures 5.19e and 5.19f show those for DD2. The three cases are very similar before 1800, where the influence of the long data gaps dominates. After 1800 the uncertainty in the total flux is lower for smaller CO_2 uncertainties and the uncertainty in the biospheric flux is higher for larger $\delta^{13}C$ uncertainties, as would be expected. This type of calculation gives an indication of how precise the measurements need to be to constrain the sources to a particular level of uncertainty.

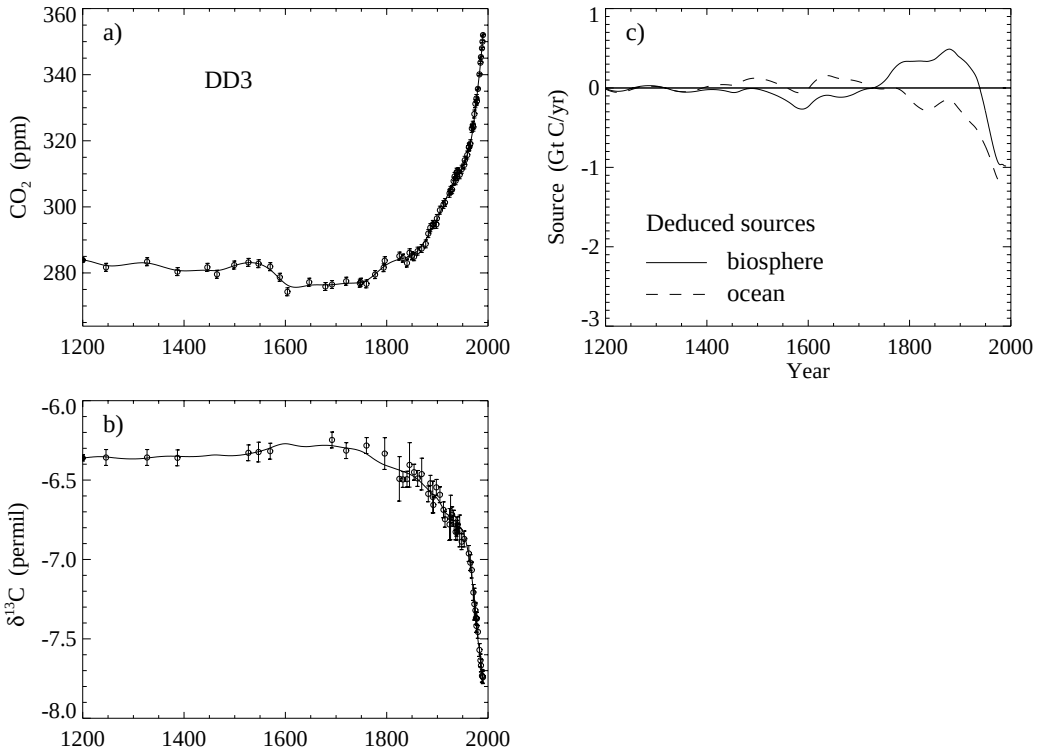

Figure 5.18: CO_2 concentration, $\delta^{13}C$ and deduced sources from the Kalman filter run with mixed layer pulse response functions, with $\mathbf{Q} = 0.001$ for both source components and published CO_2 uncertainties and doubled $\delta^{13}C$ uncertainties. This calculation is referred to as DD3.

Smoothing on ice core air due to the firn processes is about 18–20 years for DSS (Section 3.7.1) but the sampling density is quite a lot less than this in the pre-industrial part of the record. It is proposed that in the future, more measurements will be made to increase the sampling density for the Law Dome ice cores. A feature of the Kalman filter (as well as other linear least squares-like estimation problems) is that estimates of the state covariance do not depend on the data values, only on prior error covariances (Gelb, 1974, p110; Wunsch, 1996, p381). This means that the KFDD can be run with dummy CO_2 and $\delta^{13}C$ data at increased density to estimate the source uncertainties that could be expected for such a data density. Although this application is slightly non-linear, the use of dummy CO_2 and $\delta^{13}C$ measurements from spline fits to the ice core records should mean that the results of this test are realistic. Figure 5.20a shows the flux error variances for a data spacing of 10 years through the entire record and the published data

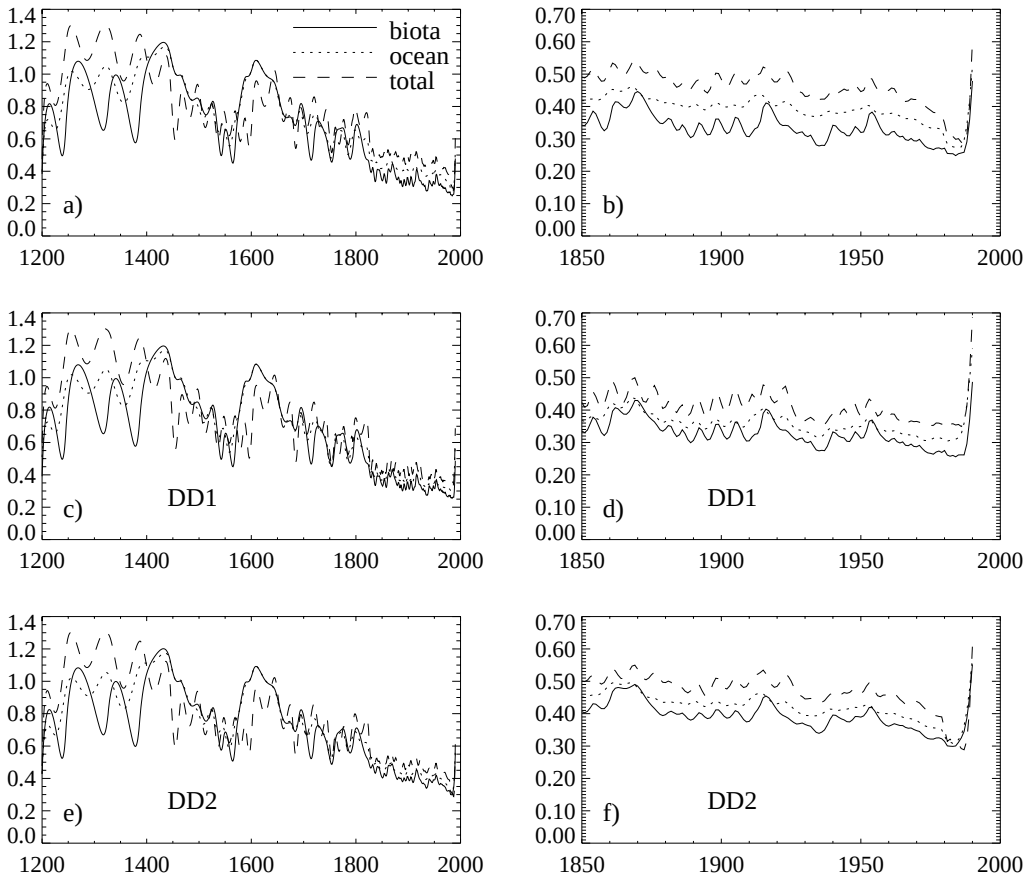

Figure 5.19: Source uncertainties (GtC yr^{-1}) from the MLRF double deconvolution. a) and b) show the results using the published data uncertainties from Etheridge et al. (1996) and Francey et al. (1999a). c) and d) show the uncertainties for DD1 (which uses reduced CO_2 uncertainties and published $\delta^{13}C$ uncertainties) and e) and f) are for DD2 (published CO_2 uncertainties and increased $\delta^{13}C$). All three cases use $\mathbf{Q} = 0.1$ (GtC $yr^{-1})^2$.

uncertainties of 1.2 ppm and 0.025 ‰ for CO_2 and $\delta^{13}C$ respectively. Figure 5.20b shows the flux uncertainties for the same data uncertainties but with data spacing of 1 year. The biospheric flux is still known better than the total flux for these data uncertainties for both data densities. Figure 5.20c shows flux uncertainties for a CO_2 uncertainty of 0.6 ppm, $\delta^{13}C$ uncertainty of 0.025 ‰ and data spacing of 1 year. For a $\delta^{13}C$ data uncertainty of 0.025 ‰, the CO_2 uncertainty needs to be below 0.3 ppm for the total source to be known as well as the biospheric source (with $\mathbf{Q} = 0.1$ (GtC $yr^{-1})^2$ and data spacing of 1 year).

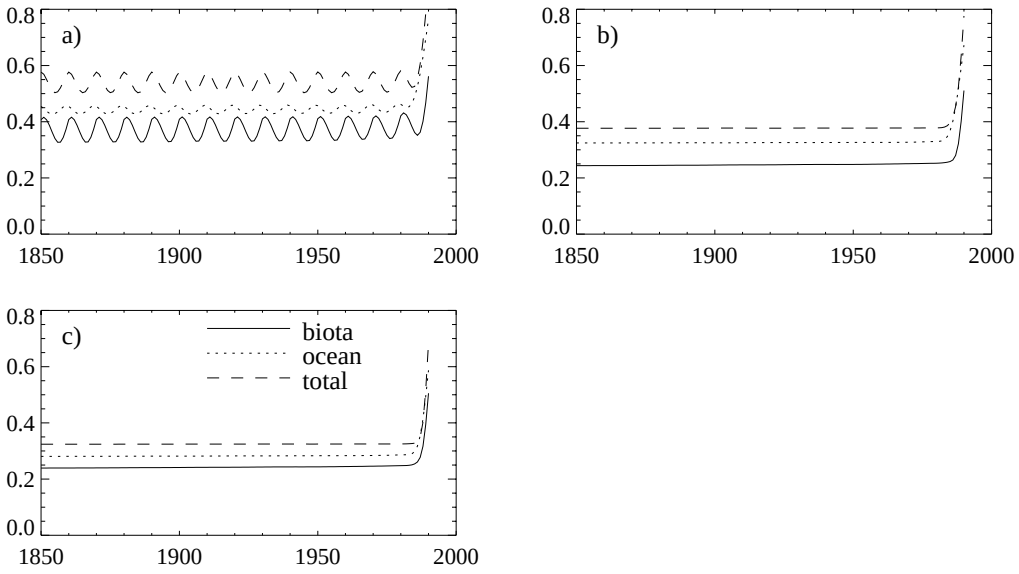

Figure 5.20: a) Source uncertainties (GtC yr^{-1}) for the MLRFDD with data spacing of 10 years throughout the entire record and CO_2 and $\delta^{13}C$ uncertainties of 1.2 ppm and 0.025 ‰, respectively. b) Source uncertainties for the same data uncertainties and 1 year data spacing. c) Source uncertainties for 1 year data spacing, CO_2 and $\delta^{13}C$ uncertainties of 0.6 ppm and 0.025 ‰, respectively.

5.8 Comparison between the Kalman filter double deconvolution and the mass balance method

The mass balance double deconvolution method (described in Section 2.10) estimates net biospheric and oceanic fluxes from the derivatives of curves fitted to CO_2 and $\delta^{13}C$ observations using mass balance. The calculation is very sensitive to the amount of smoothing chosen for these curves, as this determines the derivative and therefore the calculated fluxes. Most applications of this method (e.g. Francey et al., 1995b; Joos and Bruno, 1998) have used the budget equations derived by Tans et al. (1993) for C_a and $C_a\delta_a$ (equations (2.11) and (2.13)). The double deconvolution by Keeling et al. (1989a) differs in its implementation from the other studies (they used iterative methods rather than the solution of 2 simultaneous equations), however the two methods are effectively equivalent since they both require CO_2 and $\delta^{13}C$ to be known at every timestep. There are advantages and disadvantages of both the Kalman filter double deconvolution and the mass balance method, as well as some similar problems. The two methods are compared in this

section, with particular reference to the results from Joos et al. (1999) who applied the mass balance method described by Joos and Bruno (1998) to the Law Dome CO_2 and $\delta^{13}C$ ice core record.

Double deconvolution methods have been applied to direct measurements of CO_2 and $\delta^{13}C$ (Francey et al., 1995b; Keeling et al., 1989a) as well as to ice core measurements (Joos and Bruno, 1998; Joos et al., 1999). The two cases have somewhat different characteristics – direct measurements generally have good temporal resolution while the ice core measurements are smoothed due to the trapping processes and often have quite sparse temporal coverage. The focus here will be on double deconvolutions for inverting ice core data.

Choice of the degree of smoothing on the CO_2 and $\delta^{13}C$ splines is important for the mass balance double deconvolution (MBDD). In a similar way, the Kalman filter double deconvolution (KFDD) needs the stochastic forcing $\mathbf{Q}$ to be specified. In a sense, the smoothing on the splines dictates how much CO_2 concentration and $\delta^{13}C$ vary with time, whereas specifying the values of $\mathbf{Q}$ in the random walk part of the Kalman filter controls the variation of sources with time. Although the two are closely related, there are advantages to specifying variation of the source rather than that of CO_2 and $\delta^{13}C$. At first thought it probably seems that it would be better to estimate variability of concentrations rather than sources, because CO_2 and $\delta^{13}C$ are actually measured, and the sources are not. However, the MBDD may have a problem if the degree of smoothing for CO_2 is not consistent with the smoothing for $\delta^{13}C$. The units for $\delta^{13}C$ are quite different to those for CO_2, and as already discussed, the atmospheric levels of each quantity respond rather differently to the uptake and release of biospheric and oceanic CO_2. In the mass balance method, splines are generally fitted separately to the CO_2 and $\delta^{13}C$, without consideration of how a particular flux influences both CO_2 and $\delta^{13}C$. The smoothing constraints for the MBDD and KFDD are also different types of constraint. The constraint on the spline controls the 2^{nd} derivative of the spline whereas the Kalman filter constrains the annual step in the random walk model. The uncertainties in the observations are used directly in the Kalman filter (i.e. matrix $\mathbf{R}$). In the mass balance method, they can be used to give a weighted spline or more qualitatively to help determine smoothing of the splines.

The Kalman filter allows a more rigorous analysis of the statistics, and the relationship

between CO_2, $\delta^{13}C$ and the two net fluxes. Because the Kalman filter includes the statistics in the calculation, rather than as a pre-processing stage, it can help to ensure that variations in CO_2, $\delta^{13}C$ and the fluxes are consistent. Specifying $\mathbf{Q}$ sets the maximum amount the source *can* vary, whereas the spline gives how much the CO_2 and $\delta^{13}C$ *do* vary. Specifying a larger value of $\mathbf{Q}$ will allow, but not force, the source to vary by a larger amount from one year to the next. If, for example, it was believed that the biospheric flux was more variable than the oceanic flux, the KFDD could model this with a larger element of $\mathbf{Q}$ for the biospheric than oceanic flux. The KFDD would then assign appropriate uncertainties to the deduced fluxes. Modelling this with the MBDD would be difficult. A closer fit to $\delta^{13}C$ measurements with the MBDD wouldn't achieve this, as it could cause anticorrelated fluxes. Joos et al. (1999) used Monte Carlo simulations to estimate uncertainties on the net fluxes due to uncertainties in the ice core data. The flux uncertainties estimated with the MBDD by Joos et al. (1999) are the same for the biospheric and oceanic fluxes (Joos and Bruno, 1998). The different uncertainties on the ocean, biospheric and total fluxes in the Kalman filter have already been demonstrated.

Missing data is not a problem for the Kalman filter, as the correction step is only performed when observations are available. The fact that interpolation is not required in the Kalman filter is a particular advantage for the ice core application. Even though the state will not be well constrained when there are gaps in the data, the best estimate should come from the state space model. Interpolation of concentration prior to filtering would impose a solution that may not be correct. In data gaps, the uncertainties increase as evolution continues without comparison with data. The Kalman smoother will improve the state estimates near the end of a large data gap compared with the forward pass.

Perhaps the most striking advantage of not having to interpolate is when there is a CO_2 measurement but no corresponding $\delta^{13}C$ measurement (or vice versa). The Kalman filter is able to use the CO_2 measurement but make no assumption about the $\delta^{13}C$ at this time, letting it continue to evolve until there is data available. The spline method will fit a smooth curve through the data gap, making assumptions about $\delta^{13}C$ at the time of the missing point which are not necessarily consistent. This can be seen around 1600, where there is a CO_2 measurement but no $\delta^{13}C$. The CO_2 value is the lowest for the entire Law Dome record, and without a corresponding $\delta^{13}C$ measurement it is difficult to attribute

a cause. The Monte Carlo analysis as described by Bruno and Joos (1997) performed by perturbing existing data points is unlikely to give the real range of δ^{13}C values that may have occurred at this time, so the uncertainties estimated by the MBDD may not reflect the actual uncertainties. The KFDD has a fairly small uncertainty on the total source around 1600 but large uncertainty on the biospheric and oceanic fluxes separately. Joos et al. (1999) fits quite a smooth spline to the pre-industrial data (spline cutoff of about 300 years) so the low 1604 CO_2 value is not closely fitted. Their δ^{13}C spline through this period is very smoothed compared to the δ^{13}C from the Kalman filter. The characteristic of the KF uncertainties being maximum in the middle of long data gaps is probably not shared by the MB calculation.

Both methods can get spurious anticorrelated fluxes if something is wrong. The KFDD may get anticorrelated sources if the data, uncertainties or assumptions are wrong, although there are checks that can be made on the statistics (e.g. χ^2, normalised residuals). The MBDD may get anticorrelated fluxes if the CO_2 and δ^{13}C splines are not consistent.

The MBDD calculation by Joos et al. (1999) and KFDD calculation use similar underlying carbon cycle models. Joos et al. (1999) use a 4-box biosphere and the HILDA ocean model (mixed layer response function form) for calculating the isofluxes. Sensitivity studies for the isofluxes are relevant to both calculations. In both calculations, the deduced oceanic flux is not necessarily consistent with the modelled ΔpCO_2 (Joos and Bruno, 1998).

It would be possible in the KFDD to include a range of additional information. For example, information on climate variations could be included using 'observations' of the sources, perhaps with large uncertainties. Measurements of mixed layer δ^{13}C, such as from the sponge records of Böhm et al. (1996; 2000) could be used. It is harder to see how this could be done with the MBDD.

5.9 Concluding remarks

In this chapter, a method for performing a double deconvolution calculation on ice core data has been developed. The calculation incorporates statistical analysis with a standard carbon cycle model using a statistical technique known as the Kalman filter. Application of the Kalman filter to ice core measurements was demonstrated for methane with a sim-

ple model. Then two different Kalman filter double deconvolution methods for CO_2 and $\delta^{13}C$ were developed. The first method, using atmospheric pulse response functions, was a simple model, and as such suffered from small inaccuracies due to the simple approximations. Nevertheless, it proved to be a useful demonstration of the calculation. The second model, using mixed layer pulse response functions, was more complicated and physically correct. The Kalman filter double deconvolution calculation estimates the net biospheric and oceanic fluxes of CO_2 and their uncertainties. A key input to the calculation is the parameter $\mathbf{Q}$, that controls the maximum variation of the sources with time.

Three standard double deconvolution calculations were identified, DD1, DD2 and DD3. DD1 and DD2 both used the value of $\mathbf{Q}$ suggested by the firn model for CO_2 variations that survive firn smoothing and bubble trapping. DD1 used data uncertainties that could be described as optimistic and pushing the data to its limits. DD2 used more conservative data uncertainties. DD3 captures century time scale variations with a small $\mathbf{Q}$ and the conservative data uncertainties.

The Kalman filter double deconvolution method has been compared with the traditional double deconvolution method that involves fitting smoothing splines to the CO_2 and $\delta^{13}C$ data and estimating sources by mass balance. The KFDD has a number of advantages over the mass balance method. As the method combines statistical and physical models, it allows investigation of many of the statistical properties directly relating to physical quantities. The uncertainty analysis in the Kalman filter method is far superior to that generally used in the mass balance method. The Kalman filter method has better treatment of missing data than the mass balance method. It also has the ability to be extended to include a range of different types of data. The flux uncertainties are different for the oceanic, biospheric and total fluxes, reflecting variations in data density and the information about net fluxes contained in the CO_2 and $\delta^{13}C$ measurements. The results of the Kalman filter double deconvolution calculations will be discussed in some detail in the next chapter, in conjunction with the techniques from the previous chapters.

Appendix 5-1 : Kalman filtering notation

$\mathbf{H}_k$	projection of state onto observations ($m \times n$).
$\mathbf{L}_k$	Kalman gain matrix.
$\mathbf{P}_k$	state covariance matrix at time t_k ($n \times n$).
$\mathbf{Q}_k$	covariance of stochastic forcing, $\mathbf{w}_k$.
$\mathbf{R}_k$	covariance of measurement noise, $\mathbf{v}_k$.
$\mathbf{u}_k$	deterministic forcing.
$\mathbf{v}_k$	measurement noise.
$\mathbf{w}_k$	stochastic forcing (model noise).
$\mathbf{x}_k$	state at time t_k ($n \times 1$).
$\bar{\mathbf{x}}_k$	state estimate at k projected from $\hat{x}_{k-1}$.
$\hat{\mathbf{x}}_k$	state estimate at k projected and corrected with data.
$\hat{\mathbf{x}}_{k\|N}$	state estimate from smoother (i.e. at time t_k using data up to time t_N).
$\mathbf{z}_k$	observation at time t_k.
ν_k	innovation ($\mathbf{z}_k - \mathbf{H}_k\bar{\mathbf{x}}_k$).
Φ_k	state evolution matrix .
λ_k	auxiliary variable used in Bryson-Frazier smoother.
Λ_k	covariance of λ_k.
Γ_k	innovation covariance.
χ^2	(chi-squared) statistic.